2

CFD Investigation of Aerodynamic Effects on Multi-span Low-rise Structures with Curved Canopy Roofs of Different Apex Height

Agyeya Mishra, Atulya Verma, Ayush Ranjan, Deepak Sharma, Ritu Raj*

Department of Civil Engineering, Delhi Technological University, Delhi, India

*Corresponding author email: rituraj@dtu.ac.in

Abstract

Several nations' wind codes have established pressure coefficients for structures with the most commonly used roof designs. However, similar work is missing for low-rise structures with curved-canopy roofs and all sides open to the wind environment. Therefore, this work investigates wind impact on single-span and multi-span low-rise structures with curved canopy roofs and an open wind environment on all sides. Ansys CFX is used to establish the wind flow pattern, conduct the simulations, and compute wind pressure coefficients on the roof of six different structures represented as a 1:50 scale model and simulated for four wind directions ranging from 0° to 90° at 30° intervals. Due to the direct head-on impact on single-span structures, pressure contours revealed positive pressure on the external face on the windward side. The external face showed suction/negative pressure for variation in incidence angle. For multi-span structures, the external face experienced suction pressure at the windward side. Positive pressure was experienced at the junction at the external face, which changed with the incidence angle. The internal face and its junction encountered positive pressure on the windward side. Negative pressure was also detected on the external face of the roof in both single-span and multi-span structures.

Keywords

ANSYS CFX; Average pressure coefficient; Computational fluid dynamics; Curved roof; Low-rise building

Received: 25 Mar 2023 | Accepted: 24 Feb 2024 | Online: 08 Mar 2024

Cite this article

Agyeya Mishra, Atulya Verma, Ayush Ranjan, Deepak Sharma and Ritu Raj (2024). CFD Investigation of Aerodynamic Effects on Multi-span Low-rise Structures with Curved Canopy Roofs of Different Apex Height. Engineering Research Transcripts, 7, 15–42.

DOI: https://doi.org/10.55084/grinrey/ERT/978-81-964105-4-4_2

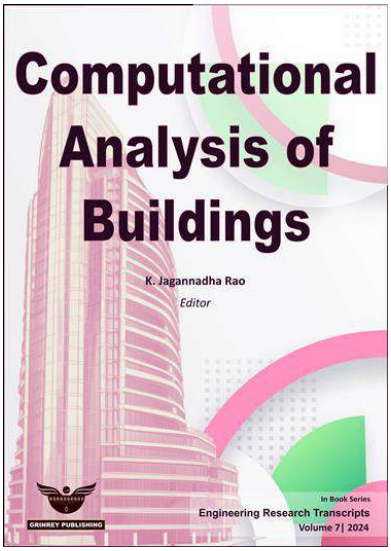

© 2024. This is an open access article and allows to use the as per CC BY-NC-SA 4.0 license.

1. Introduction

Low-rise structures are a common category of buildings that have been built recently all over the world and are utilised for a variety of uses, including residential, commercial, and industrial ones. As per IS Code 875 (Part 3): 2015, buildings that are typically built as low-rise structures are the ones that have a height of fewer than 20 meters. Buildings can be found in a variety of different landscapes and topographies, and they often come in different shapes and sizes. Wind loads can have a big influence on the structural ability of a building, particularly in areas that are prone to strong winds, such as coastal regions, open terrains, and hilltops. This is especially important in locations where earthquakes are not a major concern, as wind loads can be the primary factor influencing the lateral strength of a structure. These structures can also be divided into four categories: industrial sheds, factory buildings, warehouses, and storage buildings. In addition to these categories, there are some other special types of low-rise buildings such as the workshops where the primary purpose is to carry out repairs and maintenance of different types of vehicles, aircraft and ships. Many structures have canopy roofs that consist only of roof cladding and steel columns as support. These roofs come in a variety of shapes, such as flat, mono-slope, pitched, trough, circular, and curved. When wind flows through a structure with a canopy roof, it can impact both the interior and exterior faces of the roof. Canopy roofs may be more susceptible to damage due to wind compared to structures that have wall cladding. In addition to this, canopies have a greater surface area than walls and therefore need to be stronger to resist wind loads as compared to walls. Understanding the impact of wind on canopy roofs is crucial in the construction of this type of building. Wind can have significant effects on these structures, making it important to thoroughly study and consider these factors in the design process. The process of understanding the impact of wind on a building or structure involves three steps: (i) examining the effects of wind on the structure, (ii) determining the wind loads acting on the structure, and (iii) predicting how the structure will respond to these loads. By completing these steps, we can acquire a comprehensive understanding of the effects of wind on a building or structure. In this paper, only an investigation of aerodynamic effects on single-span and multi-span low-rise buildings has been done.

In a high-rise building, the roof faces the wind at different angles but in low-rise structures, the roof faces the wind at a single angle and the opposite side is exposed to the sheltered environment of the building. As a consequence of this, the roof surfaces of a tall building experience a higher wind load in comparison to their side walls. Numerous studies have been carried out on tall buildings. The research discussed in [1] concentrated on utilizing active control techniques to reduce wind loads on tall buildings. [2] focused on determining the reliability of computer simulations in predicting wind behaviour around high-rise buildings with complex shape and examining the role of roughness in influencing the loads due to wind acting on the building. [3] explored the impact of various structural characteristics on the horizontal displacement of the roof of a building relative to its base, the relative displacement of one floor of a building relative to the floor below it, and the bending moment at the base of tall buildings when exposed to loads due to wind. These characteristics included the stiffness of outriggers, the optimal location of outriggers, the axial stiffness of columns, and the flexibility of foundations. The research analysed how these factors affect the structural behaviour of tall buildings and their resistance to lateral loads. In order to evaluate the wind load acting on tall buildings located in an urban setting as well as their behavior to vibration due to wind, [4] utilized a combined mathematical-numerical simulation approach that involved both numerical simulation technique (CFD) and mathematical technique (FEM). This one-way coupled technique allowed them to effectively evaluate the effect of wind on these structures. [5] focused on analysing the wind-induced interference effects under various conditions and aimed to provide a detailed understanding of how wind behaviour is affected by the presence of other tall buildings. [6] focused on understanding the effects of random, chaotic fluctuations in the wind speed as well as the direction on the behaviour of tall buildings when exposed to extreme winds.

There have been numerous studies that have involved experiments aimed at analysing the effects of loads due to wind on low-rise buildings with diverse shapes & sizes, discovering that differing building plan forms and wind flow circumstances can result in radically distinct wind actions. Some of those studies are as follows: [7] aimed to understand how openings influenced the wind behaviour of low-rise buildings and how they affect the internal pressures within the buildings. [8] discussed more accurate and realistic simulation methods for wind tunnel testing of low-rise buildings. [9] developed a model to help predict the wind behaviour of low-rise light and residential buildings and to provide insight into how internal pressures may vary over time and under different conditions. [10] analysed different methods for the assessment of wind loading, utilizing the Gust Effect Factors for low-rise buildings. [11] specifically examined the downwash effect of a typical RTS on the way that the wind can alter the direction and spread of a plume emanating from a building. [12] devised a method for finding the distance over which a turbulent flow of air becomes attached to the surface of an object after separating from it, on the rooftops of low-rise buildings. [13] aimed to identify the characteristics of pressure distribution due to wind on the roofs of these structures and to examine how it varies across different locations on the roof. [14] found that all of the roof improvements examined were efficient in considerably lowering these suctions.

Several researchers have also tried to study the effects of different shapes and cross-sectional areas in low-rise and high-rise structures. Some of the most influential works include: [15] aimed to understand how the shape of a building can influence its wind loads and structural performance, and to identify the effects of different building shapes on wind loads. [16] worked on developing strategies for optimizing the shape and design of buildings in order to decrease wind loads and improve their structural performance in windy environments. [17] analysed factors such as angle of wind incidence and width of the passage affected the wind behaviour of cross-shaped high-rise buildings and to identify strategies for mitigating wind loads at re-entrant corners. Works such as [18], [19] and [20] have also tried to investigate the impacts of different roof shapes such as pitched roofs, pyramidal roofs, flat roofs, circular roofs and rectangular roofs on wind load and structural behaviour of low-rise buildings.

Wind tunnel testing is an experiment which is widely used across academia to investigate wind-induced effects on structures as well as to calculate the coefficient of pressure. Some of the most influential works include: Wind tunnel investigation methods were employed in the study [21] to investigate the wind behaviour of the membrane structure canopy roof and discover parameters that might impact its wind loads and structural performance. [22] investigated how different roof and facade shapes can affect the wind behaviour of street canyons and to identify strategies for optimizing these parameters in order to enhance the wind resistance of buildings in these environments. To generate realistic scale models of thin structures that are frequently open and have organic curves can be challenging, time-intensive, and costly. [23] presented a method for fabricating wind tunnel models of doubly-curved thin-shell structures, which included the integration of pressure sensors to facilitate experimental investigations of wind load distributions on such structures. This technique might be beneficial for researching the wind behaviour of these buildings and determining how wind loads are distributed over their surfaces. A study proposed a novel model for the assessment of discharge coefficient and flow angle at an inflow opening for cross-ventilation, with potential application in predicting the performance and optimization of cross-ventilation systems in buildings, as described in [24]. Another study, as described in [25], aims to conduct wind tunnel experiments on small-scale groups of tanks to evaluate the pressure patterns caused by group effects. A study conducted by [26] aimed to investigate the effect of wind direction on the wind loads acting on a reflector and to identify any patterns or trends in the pressure distribution across the surface of the reflector.

Although, wind tunnel testing is an experimental way of getting accurate results, its setup is very time-consuming and expensive. One can also use Computational Fluid Dynamics (CFD) to determine the coefficient of pressure values. It is a more convenient and cost-effective alternative to traditional

experimental methods, such as wind tunnel testing, which may be more time-sensitive and very costly. CFD simulations have been used in a variety of research studies to date. Some are as follows: [27] reported a thorough research of wind drags on high-rise structures of varied forms using CFD. [28] carried out CFD analysis for octagonal tall buildings considering the same parameters as used in the experimental study. Although uncommon, works such as [29] have also attempted to use other software packages such as ETABS 2015 for preparing and analysing wind load on a total of fifteen building models. A very unique approach was also taken by [30] which presented a method for predicting right usage of natural ventilation strategy that relies on the wind to provide fresh air to a building, employing both wind tunnel experimentation & CFD analysis.

There has also been a very strong critical assessment of criteria for load due to wind in IS 875 (Part 3): 2015 [31], and appropriate regulations have been adhered to at different phases throughout the study.

In this paper, aerodynamic effects on single-span and multi-span low-rise structures with curved canopy roofs and an open wind environment on all sides are studied by employing Ansys CFX for CFD software, which is used to run the simulations and determine the wind pressures on the internal and external faces of the model. This CFD study will help us calculate the average coefficient of pressure at the external and internal faces of the model as well as arrive at critical conclusions regarding the aerodynamics effects which are induced on a low-rise structure having a curved canopy roof due to load applied by the wind.

2. Structure under study

In the present study, an instrumented model of a low-rise rectangular plan of dimension 400 mm length and 200 mm breadth, curved roof structure model with apex heights 10 mm, 20 mm, and 30 mm is considered on a 1:50 geometric scale. Six columns are taken into account for the analysis of height 150 mm. The thickness of roof used is 10 mm. To investigate and understand the impact of wind on a canopy roof, the effects of wind coming from four different directions: 0°, 30°, 60°, and 90° were evaluated. These tests were performed on both single-span and multi-span models having canopy roofs. This helped us to better understand how wind direction can influence the behaviour of these structures.

To simplify the analysis, the models were exposed to a constant wind speed of 10 m/s as the structure is not very tall and the wind flows around it within the atmospheric surface layer zone, where a uniform velocity profile can be assumed. The details of the structural model are given in Fig. 1.

3. Numerical Simulation Methodology

The study investigates the aerodynamic effects on low-rise single-span and multi-span structures with curved canopy roofs. In order to do this, the ANSYS CFX Fluid Flow software was used. This software was employed to replicate the airflow around the structure and study as well as calculate the resulting forces that are applied to it. By understanding the aerodynamic forces that are acting on the structure, it becomes feasible to design the structure in such a manner that it can resist or withstand these forces.

Fluid flow is a very important aspect in the field of aerodynamics. It can be said that fluid flow is the movement of a fluid from one point to another. The fluid can be in a gaseous or liquid state. The study of fluid flow is very important in many fields such as aerodynamics, hydraulics, and many others.

ANSYS CFX is a powerful fluid flow software that is used by engineers to simulate and optimize the performance of their designs. This software has the ability to simulate various kinds of fluid flow, including laminar and turbulent, compressible and incompressible, and multiphase flow.

The 3D modelling software AutoCAD was utilized to model the structure being examined. The model was then exported to ANSYS for further analysis. ANSYS CFX is a convenient tool for simulating wind flow around bluff bodies through computational fluid dynamics. As a result, ANSYS 2022 R2 CFX fluid flow package simulations for the current inquiry are carried out utilizing the k-ϵ turbulence model at high turbulence intensity.

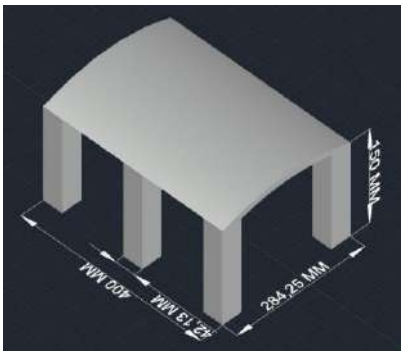

(a) Single-span structure with apex height of roof as 10 mm

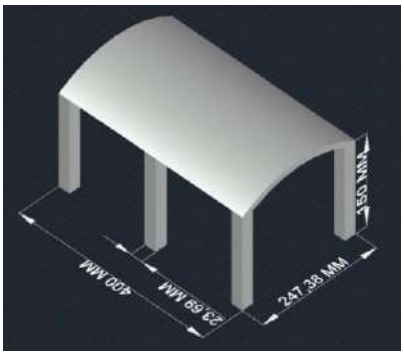

(b) single-span structure with apex height of roof as 20 mm

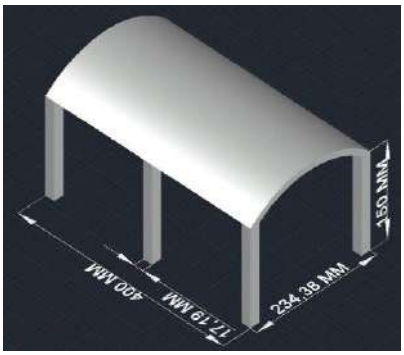

(c) single-span structure with apex height of roof as 30 mm

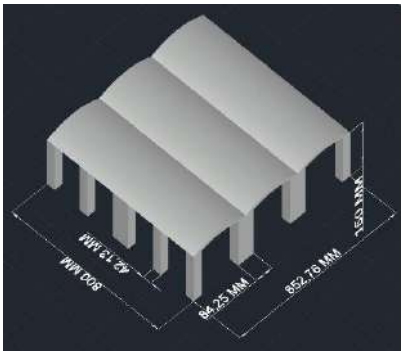

(d) multi-span structure with apex height of roof as 10 mm

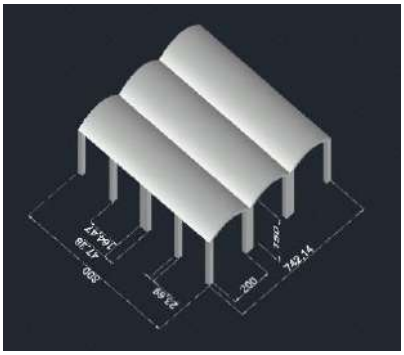

(e) multi-span structure with apex height of roof as 20 mm

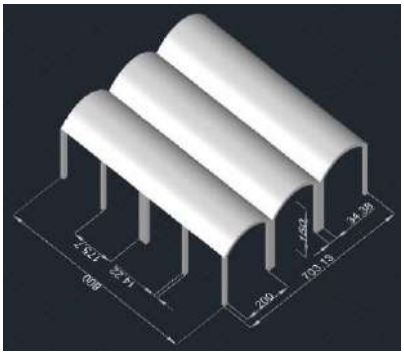

(f) multi-span structure with apex height of roof as 30 mm

Fig. 1. AutoCAD Isometric models of single-span and multi-span structures with varying apex heights

Six fundamental steps are used in CFD simulations, and they are as follows:

1. Domain and Creation of Geometry Models
2. Meshing
3. Physical Environment Configuration
4. Inlet Velocity
5. Generation of Results and Solutions
6. Mathematical Models and Equations

3.1. Domain and Creation of Geometry Models

The pre-processing stage involves setting up the computational domain as a fluid body and creating a solid body model of the flat canopy roof structure. To generate a simulated wind tunnel, a fluid flow domain should then be created around the structure. This was accomplished using Ansys' Design-Modeler tool. The experimental model dimensions are used to determine the solid body model's dimensions. In the study, the building model was not placed at the centre of the domain. Instead, it was positioned 15 times the height of the building (H) away from the inlet, sidewall, and top bounds of the domain, while the outlet boundary was 5H away. This arrangement was chosen in order to ensure that the wind flow around the building model was representative of realistic conditions and to avoid any artificial influences that might distort the results. This is carried out to guarantee proper flow around the model and avoid recirculation. The diagrammatic representation of the model of the domain is shown in Fig. 2.

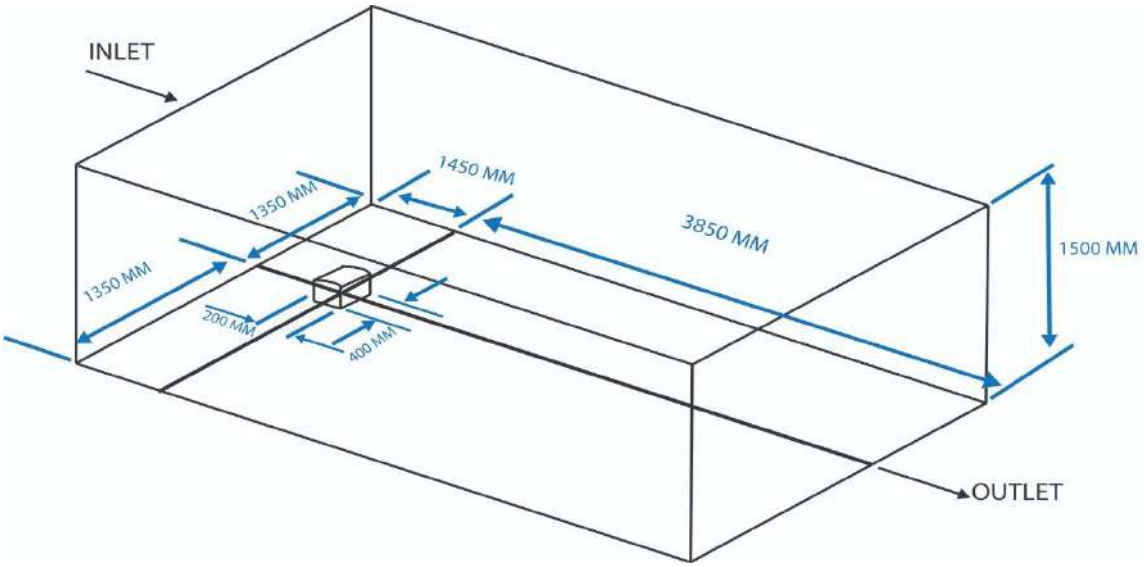

Fig. 2. Model of the domain

3.2. Meshing

The process of dividing a building model into smaller sections or parts, known as meshing, is a crucial aspect of computational fluid dynamics (CFD) simulations. Accurate meshing helps to capture the flow properties of the model with greater precision. In this study, tetrahedron meshing was used for both the domain and the building model. Tetrahedron meshing is chosen because it is faster and requires less computing power than other types of meshing. In addition, a finer edge meshing was used in important areas to capture flow parameters more accurately. The mesh size for the faces of the model was set at 0.0125 m, for edges as 0.0250 m and ground as 0.050 m.

To differentiate the domain from the building model, meshing inflation was also applied at the intersection between the two. In this study, 15 inflation layers were used between the building model and the domain. Fig. 3 below shows the meshing and inflating layer made available to models.

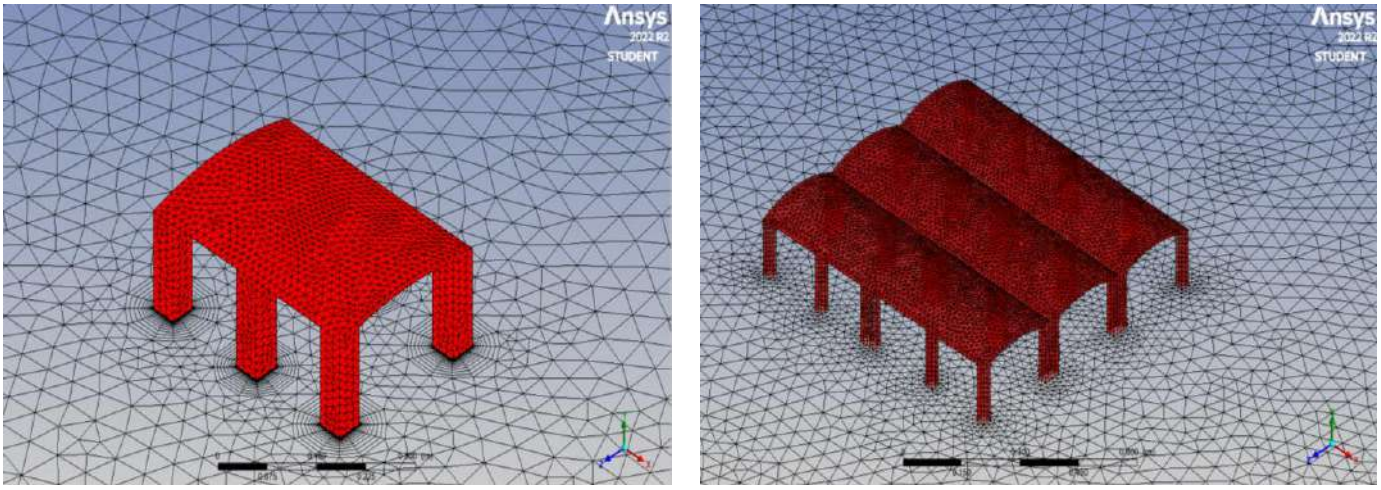

(a) (b)

Fig. 3. Mesh diagram of the model. (a) Single-span structure, (b) multi-span structure.

3.3. Physical Environment Configuration

In order to accurately model fluid flow within the computational domain, appropriate boundary conditions must be set. The boundary conditions are established by defining the wind profile and setting up the load on the inlet surface of the domain, which corresponds to the windward side. This ensures that the structure is subjected to the appropriate wind conditions. The walls of the model were classified as free-slip walls, with zero shear stress and non-zero velocity along the surfaces of the bottom, top, and side walls. To mimic the natural flow of a freestream in a virtual wind tunnel, the wall surface's normal velocity component is typically set to zero. The walls of the building model and the ground were treated as no-slip surfaces, meaning that there is no fluid velocity along the perimeter of the surface. This ensures a more accurate simulation of real-world conditions. Additionally, appropriate boundary conditions are set to account for the viscous drag or resistance encountered by the wind flow as it interacts with the ground and model surfaces. Zero pascal was used to define the relative pressure at the output.

3.4. Inlet Velocity

The inlet velocity is the speed at which the air enters the wind tunnel. Accurately knowing the inlet velocity is the first step in ensuring that the wind tunnel is modelled correctly in any CFD simulation. In this investigation, a steady and consistent velocity of 10 m/s that is the same throughout the area is introduced at the domain's inlet for the wind flow.

3.5. Generation of Results and Solutions

The next step after the user sets up the simulation in Ansys Workbench is to generate results through the Ansys Solution Manager. The Solution Manager is a tool designed to generate results for numerous types of simulations. The user can run the simulation either in batch mode or interactively. Ansys Solution Manager generates results for a simulation by retrieving the data from the simulation, running it through the Ansys solver, and then post-processing the data. The data is retrieved from the simulation by either exporting it from the simulation software or using the Ansys Solution Manager's built-in functionality to connect to the simulation software. Once the data is in the Ansys Solution Manager, the solver is run on it to generate the results. After the results are generated, they are post-processed by the Ansys Solution Manager to generate the final output.

Afterwards, an analysis of the result file to study the pressure coefficient and streamlines generated by the Ansys Solution Manager was conducted. The result file was utilized to study the pressure coefficients and streamlines at different points around the circular canopy roof. The C_p represents the ratio of pressure at a specific point to the free-stream velocity, and it is a crucial factor in determining the aerodynamic performance of a structure in the presence of fluid flow. Mathematically, pressure coefficient can be defined according to (1) given below:

$$Cp = \frac{P - P_0}{\frac{1}{2} \times \rho \times V^2} \tag{1}$$

where, P is the pressure of the wind or the force exerted by the wind on a surface at a specific location, P_0 is the reference pressure, which is used as a baseline for comparison, is the pressure in the area outside the influence of the building, such as the outlet. In this study, the reference pressure has been set to zero Pa and ρ & V are the density of air and design wind speed, respectively.

3.6. Mathematical Models and Equations

The Ansys CFX also uses a variety of different models and equations to simulate the different types of flow. The choice of model and equation will depend on the specific application being simulated. The following is a list of some important computational fluid dynamics modeling equations.

3.6.1 Navier-Stokes Equation

The Navier-Stokes equations are a set of mathematical formulae used to explain fluid motion. These are fundamental equations of fluid mechanics, which are based on the principles of mass, momentum, and energy conservation, and are used to describe various types of fluid flow such as laminar, turbulent, compressible, and incompressible flows. The Ansys CFX software, in particular, uses the Navier-Stokes equations as a foundation for simulating fluid flow, with the focus being on the conservation of momentum.

The accompanying equation can be given as,

$$\frac{\partial(\rho u_i)}{\partial t} = \frac{\partial(\rho u_i u_j)}{(\partial x_j)} - \frac{\partial}{(\partial x_j)}\left[\mu\left(\frac{\partial_{u_i}}{\partial_{x_j}} + \frac{\partial_{u_j}}{\partial_{x_i}}\right)\right] + F \tag{2}$$

where, ρ is the density of the fluid, u is the component of velocity in the respective direction, μ is the viscosity and F is the force exerted on every fluid particle.

3.6.2 Continuity Equation

The principle of mass conservation is a fundamental concept in fluid mechanics and fluid dynamics that governs the behavior of incompressible fluids. This principle is expressed through the Continuity equation, which states that the rate at which mass flows through a system is equal to the rate at which mass is conserved within that system. This equation is widely used in the analysis of incompressible fluid flows and is essential to understanding the behavior of such fluids in a variety of contexts. This equation is valid for both compressible and incompressible fluids and is widely used in the field of computational fluid dynamics (CFD), including in the Ansys CFX software. The Continuity equation is based on the laws of conservation of mass and momentum and is a crucial equation in the understanding and analysis of fluid flow.

The Continuity equation can be expressed in either a conservative or non-conservative form. The conservative formulation postulates that mass is preserved in a closed system, implying that the mass of a system stays constant over time. It also states that the mass flow rate is equal to the product of the volume flow rate and the fluid density. On the other hand, the non-conservative formulation takes into account the idea that mass is not necessarily conserved in an open system. The equation asserts that the mass flow rate can be calculated by multiplying the fluid density by the volume flow rate and the velocity of the fluid. The non-conservative form is generally considered to be more accurate and is more commonly used in computational fluid dynamics.

3.6.2.1 Conservative Form of Continuity Equation

$$\frac{\partial \rho}{\partial t} + \nabla .(\rho \vec{V}) = 0 \tag{3}$$

3.6.2.2 Non-Conservative Form of Continuity Equation

$$\frac{D\rho}{Dt} + \rho \nabla .\vec{V} = 0 \tag{4}$$

where, $\frac{D}{Dt}$ is the total derivative, $\frac{\partial}{\partial t}$ is the partial derivative, ρ is the density of the fluid, $\vec{V}$ is the velocity component of the fluid and ∇ is the divergence.

3.6.3 Bernoulli's Equation

The Bernoulli equation is a fundamental equation of fluid mechanics that is based on the law of conservation and energy and can be used to analyze and predict the behavior of fluids. It is often used in the field of aerodynamics, where it can be used to analyze the flow of air around an object. It can also be applied

to a variety of situations involving the flow of liquids and gases. In the Ansys CFX software, the Bernoulli Equation is used to simulate the flow of fluids. This allows for a better understanding of the aerodynamic effects on an object. The Bernoulli equation is a concept in fluid dynamics that explains how fluids behave under the influence of different forces. In particular, it explains how fluid pressure and fluid velocity are related. According to the principles of fluid dynamics, an increase in the velocity of a fluid is accompanied by a decrease in pressure or a reduction in the fluid's potential energy. Additionally, within a closed system, the total of kinetic energy, potential energy, and pressure energy must remain constant. This reflects the conservation of energy, which states that energy cannot be created or destroyed, only converted from one form to another. The Bernoulli equation can be used to calculate the pressure, velocity, and density of fluids in a variety of different situations.

Mathematically, it can be given as,

$$\frac{V^2}{2} + gz + \frac{P}{\rho} = constant \tag{5}$$

where, p is the fluid's pressure, V is its velocity, ρ is its density, g is gravity's acceleration and z is its vertical height above a datum level.

3.6.4 k-epsilon Turbulence Model

CFX is a computational fluid dynamics (CFD) software that is used in various industries to simulate and analyze fluid flow. The k-epsilon turbulence model is a highly popular and widely used model for predicting turbulent flow, and it is frequently employed by CFX in its simulations. The k-epsilon turbulence model is a two-equation approach that is used to forecast the energy and dissipation of turbulence in a variety of flow conditions. The versatility of this model makes it a viable choice for a wide range of applications, as it is able to handle laminar and turbulent flows, as well as both incompressible and compressible flows.

The k-epsilon turbulence model is widely utilized in the mechanical engineering domain, specifically for modelling turbulent flow in various applications such as internal combustion engines. Additionally, it is also a very popular choice in computation wind engineering (CWE) applications. The model is based on the idea that the turbulent kinetic energy (k) is transformed into heat (epsilon). It uses the turbulent kinetic energy, k, and the dissipation rate of turbulent kinetic energy, epsilon, to predict the turbulent flow field. The model includes two transport equations, one for k and one for epsilon. It is scale-dependent, meaning that the results will vary depending on the size of the computational domain. The model is suitable for turbulent flows with low to moderate Reynolds numbers.

The model is based on the conservation of mass, momentum and energy and uses the following transport equations.

3.6.4.1 Turbulent Kinetic Energy Equation

$$\frac{\partial(\rho k)}{\partial t} + \frac{\partial(\rho u_i)}{\partial x_i} = -\frac{\partial}{\partial x_j}\left[\frac{\mu_t}{\sigma_k}\frac{\partial_k}{\partial_{x_j}}\right] + 2\mu_t E_{ij}E_{ij} - \rho\varepsilon \tag{6}$$

3.6.4.2 Dissipation Equation

$$\frac{\partial(\rho\varepsilon)}{\partial t} + \frac{\partial(\rho\varepsilon u_i)}{\partial x_i} = -\frac{\partial}{\partial x_j}\left[\frac{\mu_t}{\sigma_\varepsilon}\frac{\partial\varepsilon}{\partial_{x_j}}\right] + C_{1\varepsilon}\frac{\varepsilon}{k}2\mu_t E_{ij}E_{ij} - C_{2\varepsilon}\rho\frac{\varepsilon^2}{k} \tag{7}$$

where, u_i represents velocity component in their respective directions, E_{ij} is the rate of deformation or strain rate, μ_t represent eddy velocity and $\sigma_\varepsilon, \sigma_k, C_{1\varepsilon}, C_{2\varepsilon}$ are constants.

4. Validation with Indian Standards

It is very important to validate the setup of Computational Fluid Dynamics (CFD) in order to ensure that it accurately predicts wind loads on structures. There are various ways to validate a CFD setup, but the most common and widely accepted method is to compare the CFD results with wind tunnel test data. Here, we present a method for validating the CFD setup according to the Indian Standard IS 875 (Part 3): 2015 in order to assess the adequacy of the setup.

Ansys is a computer-aided engineering software that is used for simulating various engineering processes, including fluid dynamics. A crucial aspect of any CFD simulation is the mesh, which represents the discretization of the continuous domain into a collection of small, discrete volumetric elements. The quality of the mesh is crucial to the accuracy and convergence of the simulation results. For this reason, it is important to ensure that the mesh meets certain quality standards. There are various measures of mesh quality, and the recommended values for each measure depend on the type of simulation being performed. In general, a high-quality mesh will have smaller elements near areas of high curvature or high gradient and larger elements in areas of low curvature or gradient. To accurately simulate the flow of a fluid around an object, a mesh with appropriate resolution is essential. The mesh should be refined enough to capture the details of the flow, but not so much that it results in excessively long computational times. In addition, the mesh should be as regular as possible to minimize errors and increase the efficiency of the computation.

To ensure the reliability of our outcomes, we implemented a validation model with identical internal and external dimensions and mesh settings as the flow configuration under investigation. This allowed us to verify the accuracy of our simulations by comparing the results from the validation model with those from the flow setup under investigation. To determine the appropriate size for our domain, we consulted a reference [32] on using CFD in wind engineering, which provided guidelines on this topic. This allowed us to make informed decisions about the dimensions of our domain. To ensure a consistent flow of air through the wind tunnel, we positioned the inlet and outlet faces a specific distance away from the structure. The inlet was located 5H away, while the outlet was situated 15H away. This helped to create a controlled environment for our tests. In order to allow for a sufficient flow of air around the building, we set the side and top clearance to 5H. This value was based on the height of the structure, which was 0.025 meters. By maintaining this clearance, we were able to ensure that the flow of air was not obstructed during our tests. The values for the dimensions of the domain can be found in Table 1.

Table 1. Values of dimension for wind flow domain for validation model in Ansys

Inlet	Outlet	Side Clearance	Height	Number of Inflation Layers
1350 mm	3850 mm	1450 mm	1500 mm	5

To ensure an accurate representation of the building in our simulations, we carefully considered the mesh size we used. For the front of the building, we set the mesh size to 0.0125 meters, while the mesh size near the edges of the building was increased to 0.0250 meters. This helped us to capture the details of the building's surface and its interactions with the surrounding air flow, as shown in **Fig. 4**. The mesh size for the domain ground was set to 0.05 m.

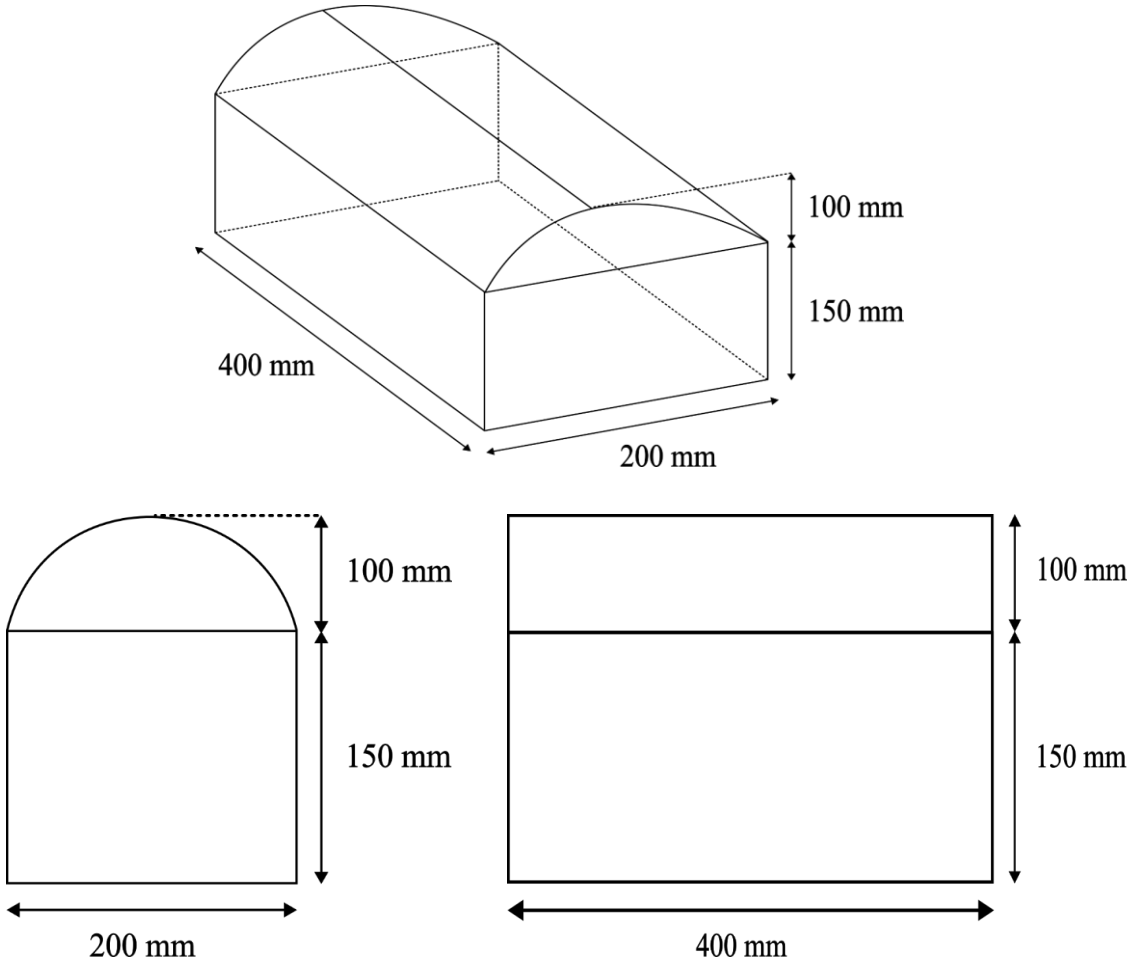

Fig. 4. Validation Model

Therefore, it is very important to have an understanding of these mesh metrics in order to produce accurate results from simulations. There are four main types of mesh metrics: cell count, aspect ratio, orthogonality, and skewness.

Cell count is a measure of the number of cells per unit volume in a simulation and determines the level of resolution at which a problem is solved. A high cell count will result in more accurate results, but a higher cell count will also increase the computational time and disk space requirements. Thus, an appropriate cell count depends on the problem being solved and the available resources. To accelerate the simulation for transient flow problems, a smaller number of grid cells should be utilized in order to decrease the computational load. Conversely, a high cell count can be used for steady-flow problems to minimize wall penetration. Most problems use medium cell counts in the range of 20-40 million cells. In a simulation, the aspect ratio is a geometric property of the cell, defined as the ratio of the largest dimension to the smallest dimension along a particular axis of a cell. It is a measure of the cell's shape and size, and it can affect the accuracy and convergence of the simulation results. Aspect ratios less than 2 usually result in a more accurate solution because the resulting meshes have fewer cells near the boundaries and are therefore less likely to suffer from boundary effects. In Ansys CFX, one can adjust an aspect ratio by changing the number of sides (or vertices) per side in their model file.

The term orthogonality is used to describe the relationship between two vectors. It is a mathematical concept which describes how points in space are related to each other. In this case, it refers to the relationship between mesh and material properties such as density, temperature or pressure. The result of using an incorrect value for these parameters can lead to poor quality meshes that fail to represent the physical phenomenon being modelled correctly. The orthogonality checkbox in Ansys CFX allows to

specify whether a mesh should be created with or without orthogonalization of its elements (i.e., whether it should be linearized).

The skewness metric is a measure of the deviation from symmetry in an object. It is calculated by taking the absolute value of the difference between two angles and dividing it by 2p (where p is equal to 360 degrees). The result will be positive if the angle that has been measured deviates more than twice as much as the other angle, or negative if it deviates less than twice as much. A high value for Skewness indicates that objects are not symmetrical and will have poor mesh quality.

There are many other factors to consider when generating a high-quality mesh, but in this section, we will focus only on recommended values by ANSYS (ANSYS Meshing User's Guide, Release 13.0. Canonsburg: ANSYS, Inc., 2010., n.d.). In order to ensure the accuracy of our simulations, we used a mesh that had excellent characteristics. Specifically, the average skewness value of the mesh was 0.34, while the average orthogonal quality was 0.76. Both of these values were within the "very good" range, indicating that the mesh was well-suited for our purposes. Additionally, in order to create a realistic simulation of wind flow, we made sure that none of the elements in our mesh fell into the "bad" or "unacceptable" range for either skewness or orthogonal quality. This helped to ensure that the flow of wind was uniform and consistent. During the simulation, the wind was directed perpendicular to the longitudinal axis of the model, which is equivalent to a 0° wind incidence according to the guidelines outlined in IS 875 (Part 3): 2015. By comparing the results in Table 2 with the values given in Table 18 of the IS 875, an average percentage error of 7.4% was measured for the whole roof.

Table 2. Validation of CFD setup according to IS 875 (Part 3): 2015

Wind Incidence Angle	Average value of C_{pe} for roof from CFD simulation	Average value of C_{pe} for roof as per IS 875 (Part 3): 2015	Percentage Error
0	-1.28896	-1.2	-7.4

As wind flows past the sharp edges of the bluff body, it creates high and strong negative pressure at the top of the roof. The CFD simulations accurately depict the pressure variations, resulting in a slightly higher average suction C_{pe}. After comparing our results to the guidelines provided in IS 875, we found that there was a difference of 0.08896 in the C_{pe} values. Despite this discrepancy, the results of our validation model met the requirements set forth in the code. As a result, we used the same meshing and boundary setup (as shown in Fig. 5) in the simulations conducted in this study. This helped us to ensure the consistency and accuracy of our results.

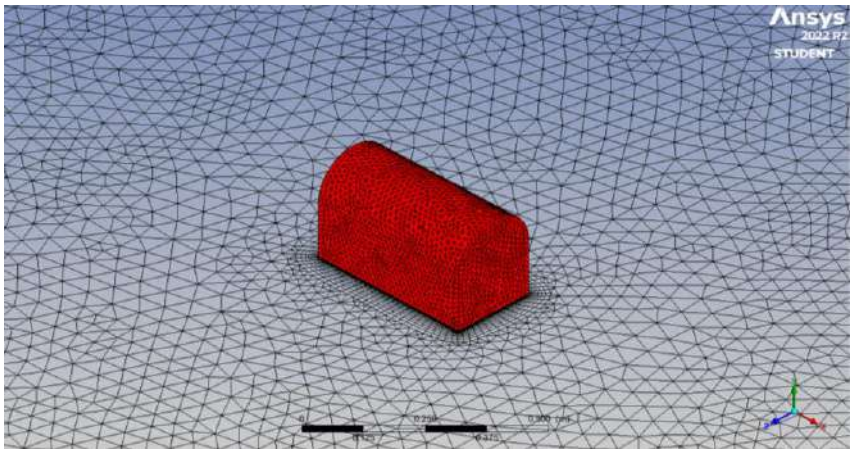

Fig. 5. Mesh diagram of Validation Model

5. Results and Discussion

A study on the pressure distribution on single-span and multi-span low-rise buildings with canopy roof surface was conducted with varying apex heights of 10 mm, 20 mm, and 30 mm.

In low-rise buildings with a curved canopy roof spanning a single span, when wind blew perpendicular to the long edge of the structure, a region of negative pressure was generated at the windward edge of the top roof surface. This suction gradually decreased as one moved towards the leeward edge.

From Table 3, it can also be seen that the edges of the surface facing the direction of the wind experienced the highest negative pressure (suction) ($C_{pe} = -0.4138$) for the 10 mm apex height model at 30°, while the 20 mm apex height model experienced the highest suction pressure ($C_{pe} = -0.3756$) at 0° and the 30 mm apex height model ($C_{pe} = -0.4845$) at 0°. Based on this, it can be concluded that the suction pressure distribution on the surface of a single-span low-rise building with a curved canopy roof is significantly affected by the height of the apex of the roof.

One can observe a gradual increase in positive pressure on the top surface as the angle of wind incidence increased from 0° to 90° in the model having a 10 mm apex height. On the other hand, the positive pressure on the bottom surface decreased gradually while the wind incidence angle increased from 0° to 90° in the model with a 10 mm apex height.

At 90° for all three models, a very low value of negative suction pressure developed. It was also observed that as the apex height of the models increased, the suction pressure experienced at the topmost point of the top surface (exterior contour) increased. This indicates that higher apex heights can provide greater resistance to wind loads and other aerodynamic forces. The pressure contours for single-span low-rise structures having varying apex heights are represented in Fig. 6-11. The velocity streamlines for single-span low-rise structures having varying apex heights are represented in Fig. 12.

The information regarding the aerodynamic effects is crucial for the design and construction of multi-span low-rise structures with curved canopy roofs of different apex height. They also indicate that the presence of a curved canopy roof on multi-span low-rise structures has a significant effect on the aerodynamic forces acting on the structure. The results for coefficient of pressure for multi-span models having varying apex heights has been represented in Table 4-6.

The model with a 10 mm apex height showed that the highest positive pressure was observed at the junction of different roofs. On the upper surface, maximum coefficient of pressure was observed at 30° on the first and third roof on the windward side, and at 60° on the second roof. The highest magnitude of suction pressure occurred at the top of the first roof. Suction pressure was observed on the lower surface at 90°, while the maximum coefficient of pressure was observed on all roofs at 0°. The positive pressure magnitude decreased gradually from the windward to the leeward side.

The model with 20 mm apex height showed similar results as the 10 mm apex height model, with the highest positive pressure observed at the junction of different roofs and maximum coefficient of pressure observed at 30° on the first and third roof on the windward side and at 60° on the second roof. However, the magnitude of positive pressure and suction pressure was slightly higher compared to the 10 mm apex height model.

The model with the 30 mm apex height showed a different pattern in the distribution of aerodynamic forces compared to the other two models. The highest positive pressure was still observed at the junction of different roofs, but the maximum coefficient of pressure on the upper surface was observed at 0° on the first roof on the windward side and at 30° on the second and third roof on the windward side. At the wind incidence angle of 0°, the entire lower roof experienced positive pressure, and its magnitude reduced from the windward to the leeward side.

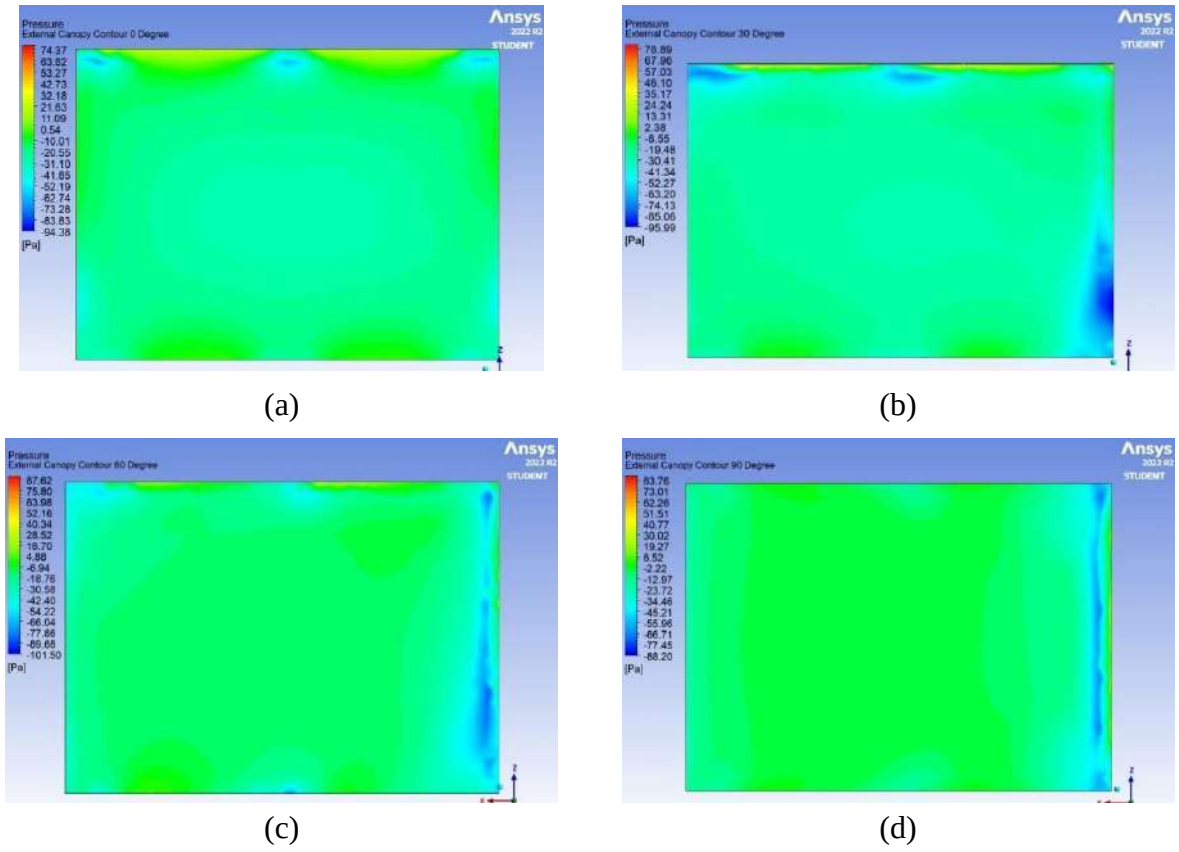

(a) (b)

(c) (d)

Fig. 6. External pressure contours for single-span low-rise structure having apex height of roof as 10 mm. (a) 0° wind incidence, (b) 30° wind incidence, (c) 60° wind incidence, (d) 90° wind incidence.

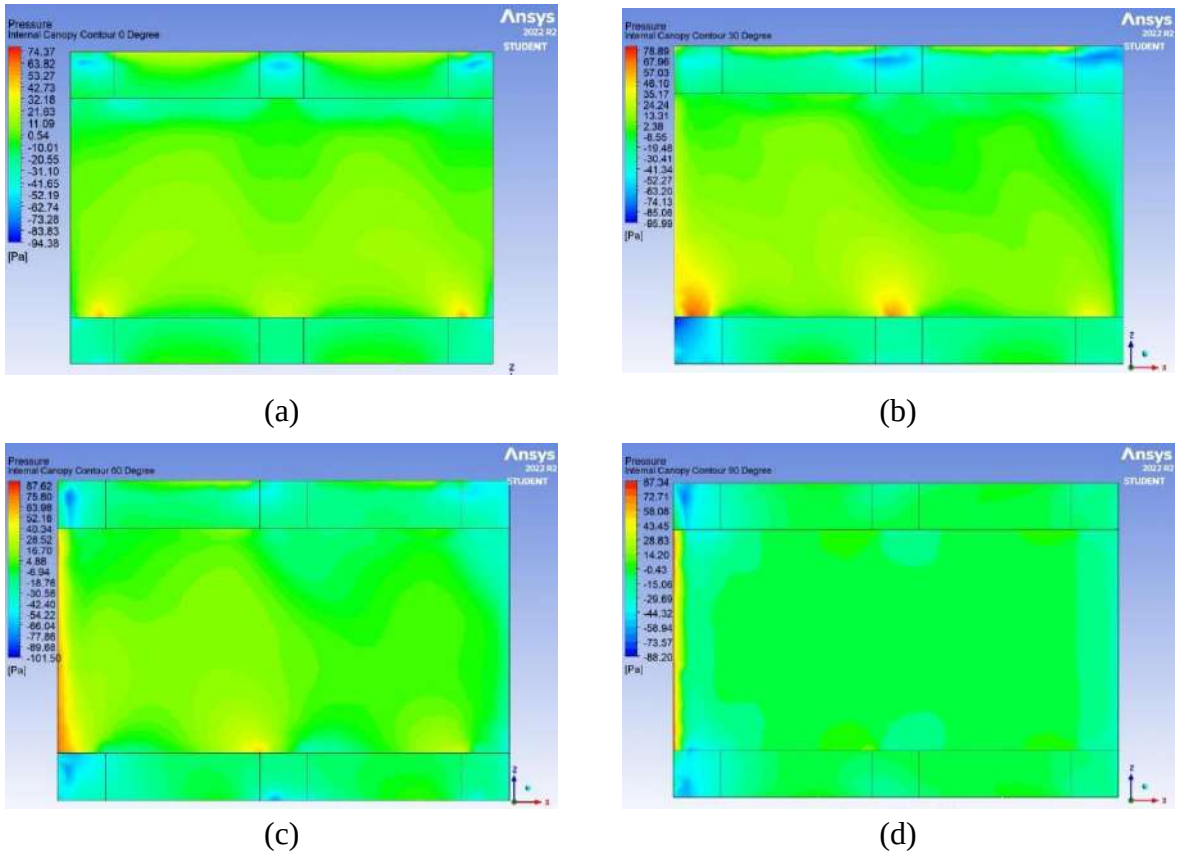

(a) (b)

(c) (d)

Fig. 7. Internal pressure contours for single-span low-rise structure having apex height of roof as 10 mm. (a) 0° wind incidence, (b) 30° wind incidence, (c) 60° wind incidence, (d) 90° wind incidence.

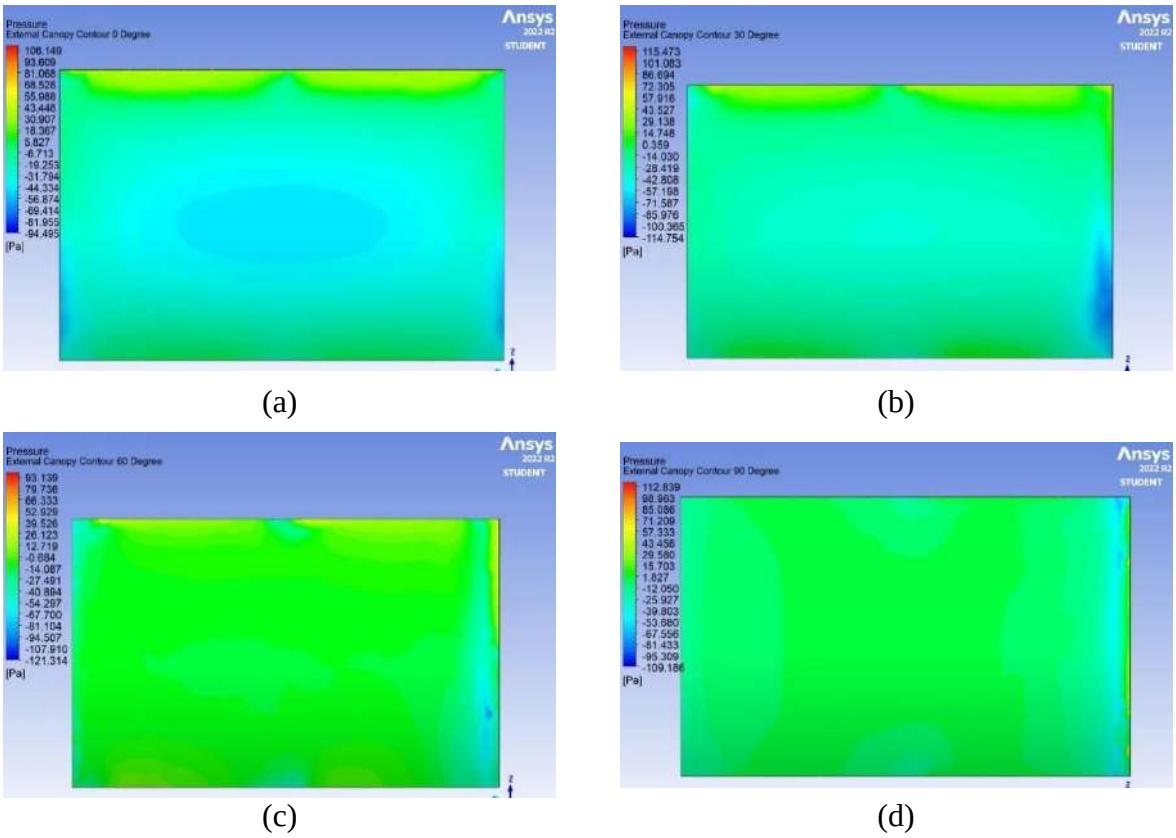

Fig. 8. External pressure contours for single-span low-rise structure having apex height of roof as 20 mm. (a) 0° wind incidence, (b) 30° wind incidence, (c) 60° wind incidence, (d) 90° wind incidence.

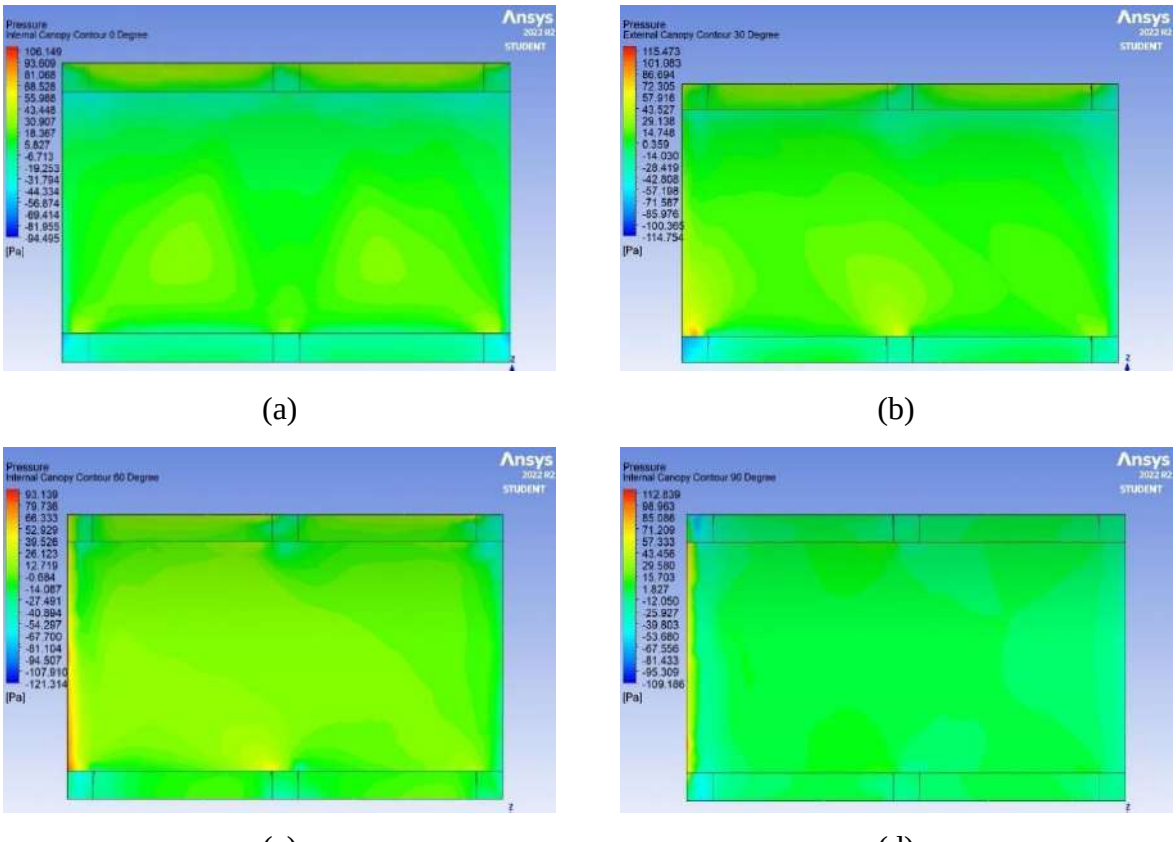

Fig. 9. Internal pressure contours for single-span low-rise structure having apex height of roof as 20 mm. (a) 0° wind incidence, (b) 30° wind incidence, (c) 60° wind incidence, (d) 90° wind incidence.

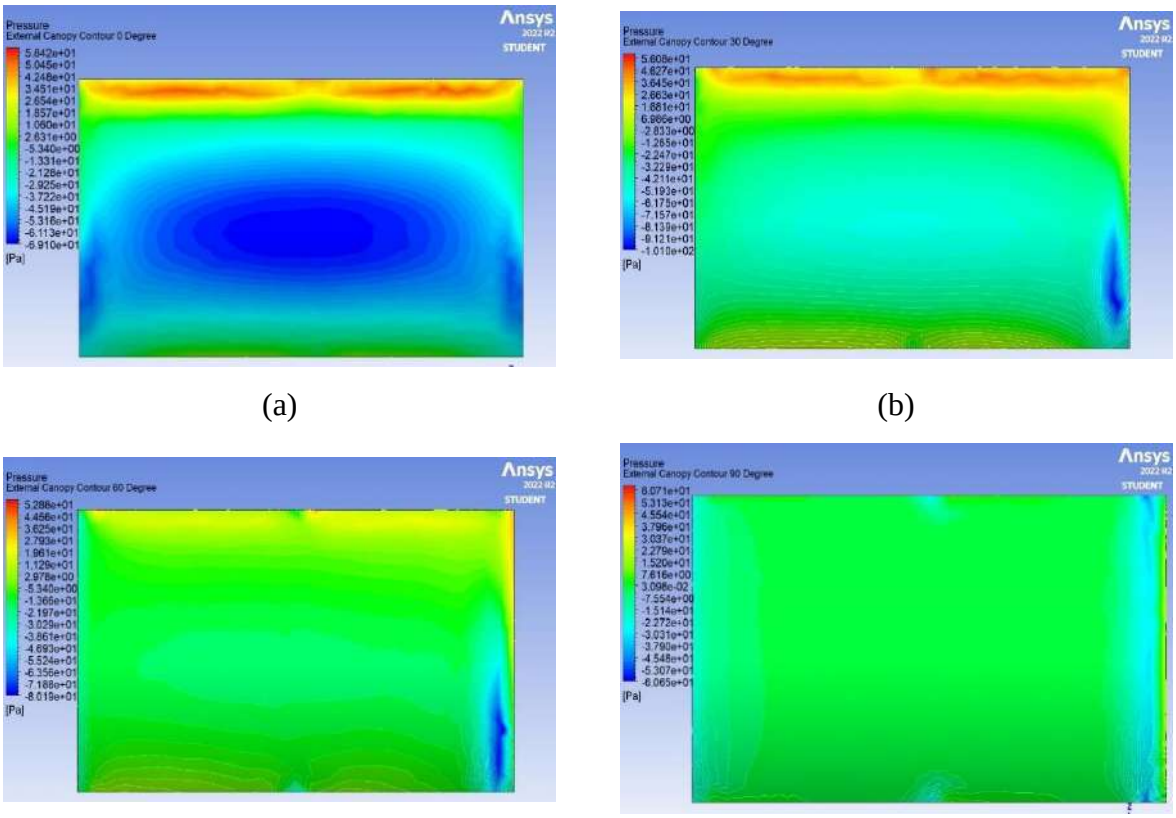

(a) (b)

(c) (d)

Fig. 10. External pressure contours for single-span low-rise structure having apex height of roof as 30 mm. (a) 0° wind incidence, (b) 30° wind incidence, (c) 60° wind incidence, (d) 90° wind incidence.

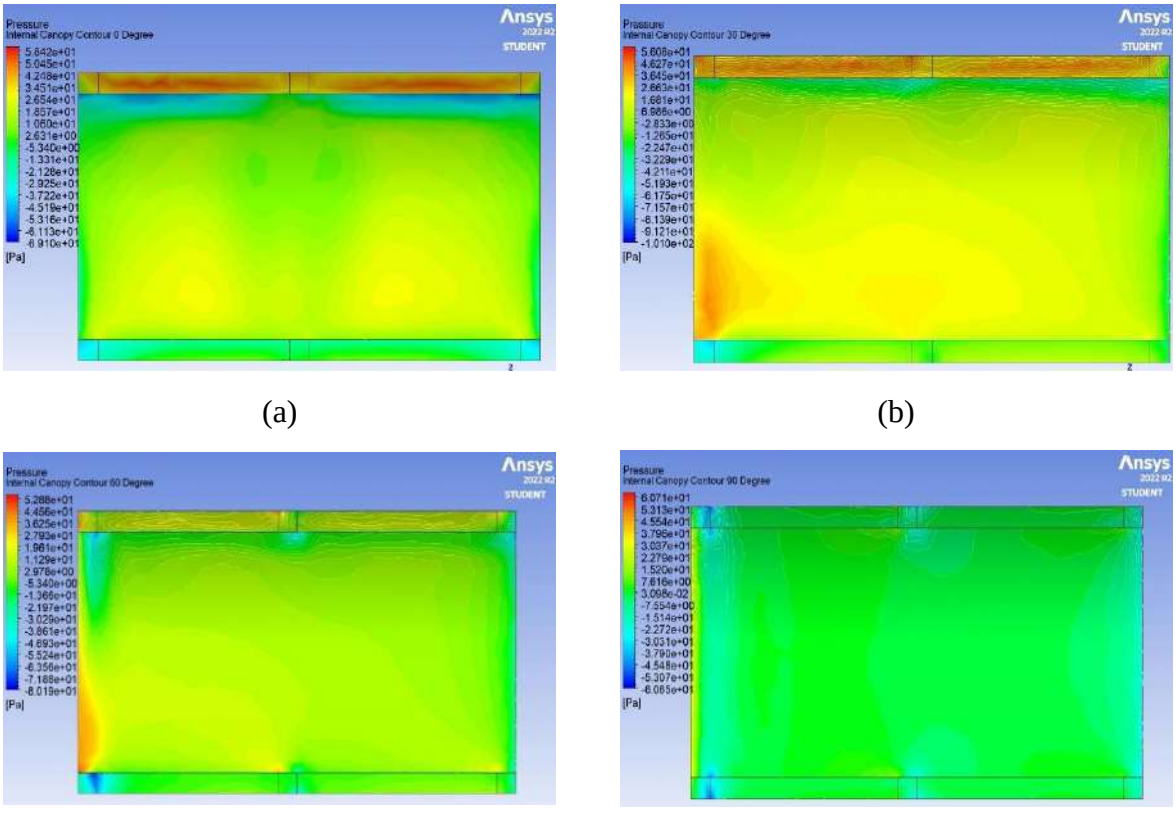

(a) (b)

(c) (d)

Fig. 11. Internal pressure contours for single-span low-rise structure having apex height of roof as 30 mm. (a) 0° wind incidence, (b) 30° wind incidence, (c) 60° wind incidence, (d) 90° wind incidence.

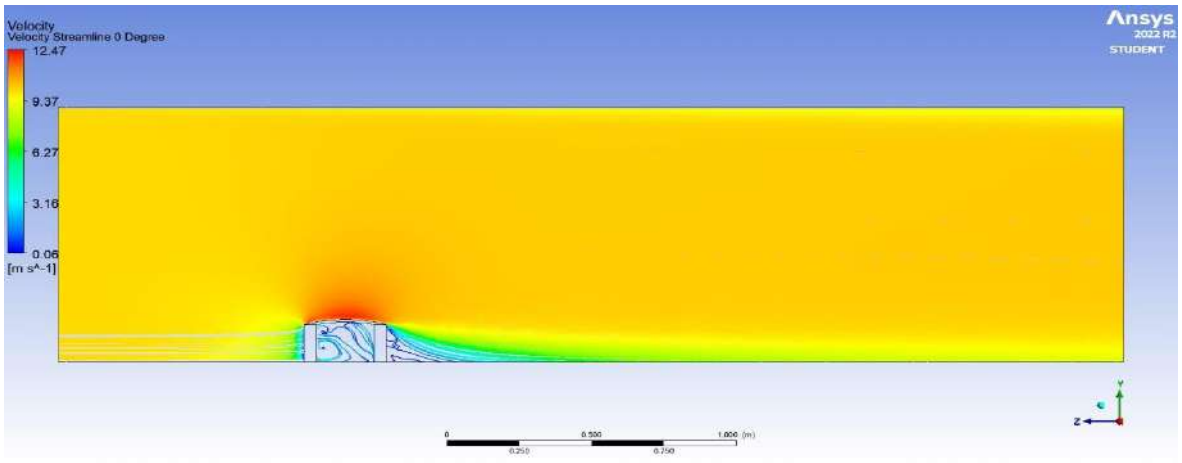

(a)

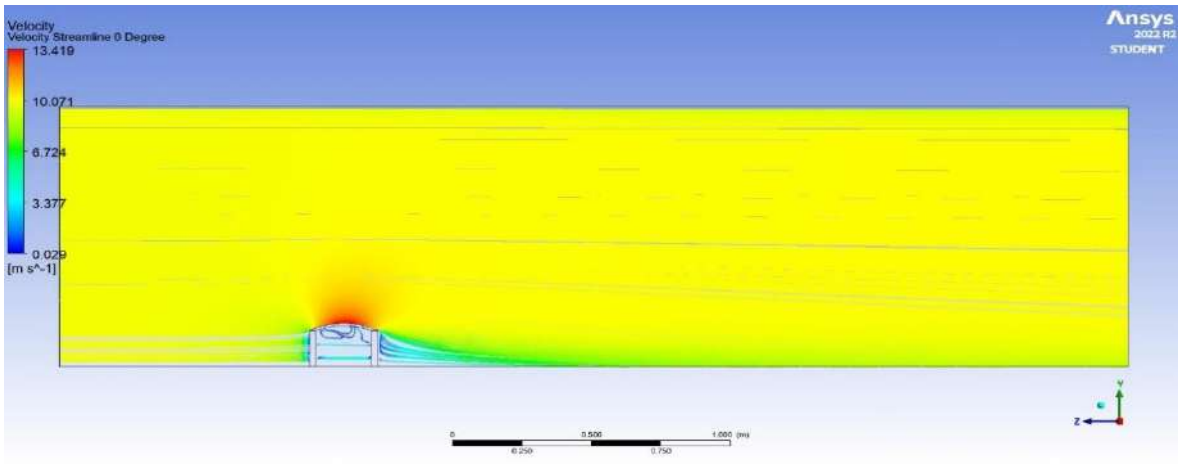

(b)

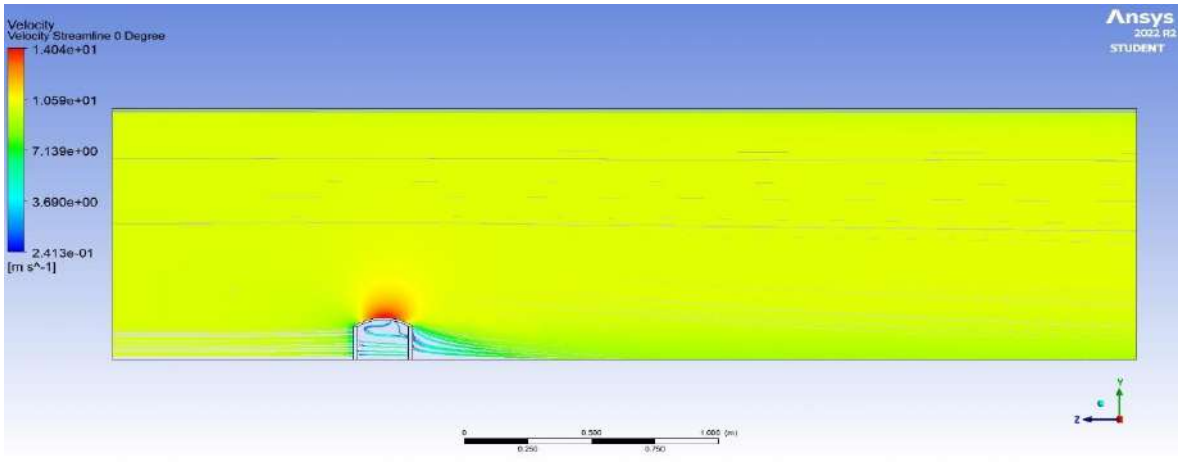

(c)

Fig. 12. Velocity streamlines for single-span low-rise structures. (a) 0° wind incidence, 10 mm apex height model, (b) 0° wind incidence, 20 mm apex height model, (c) 0° wind incidence, 30 mm apex height model.

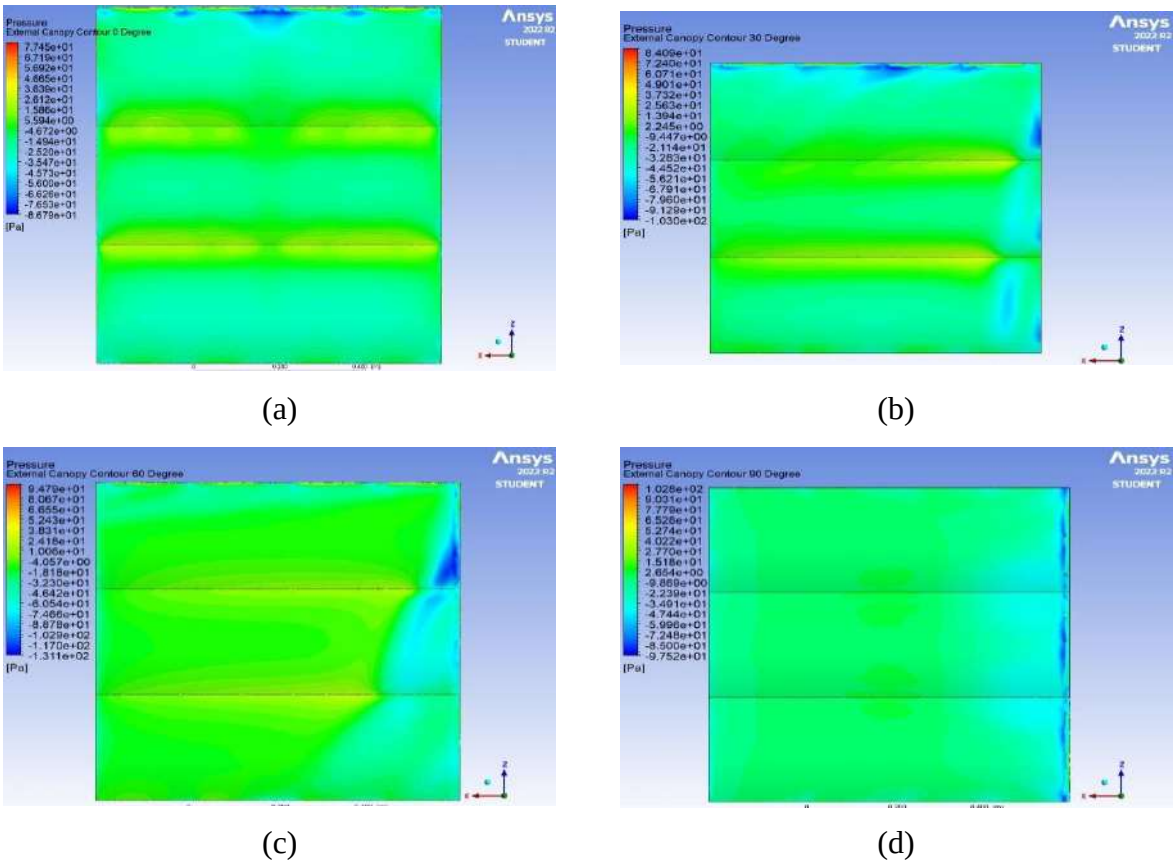

(a) (b)

(c) (d)

Fig. 13. External pressure contours for multi-span low-rise structure having apex height of roof as 10 mm. (a) 0° wind incidence, (b) 30° wind incidence, (c) 60° wind incidence, (d) 90° wind incidence.

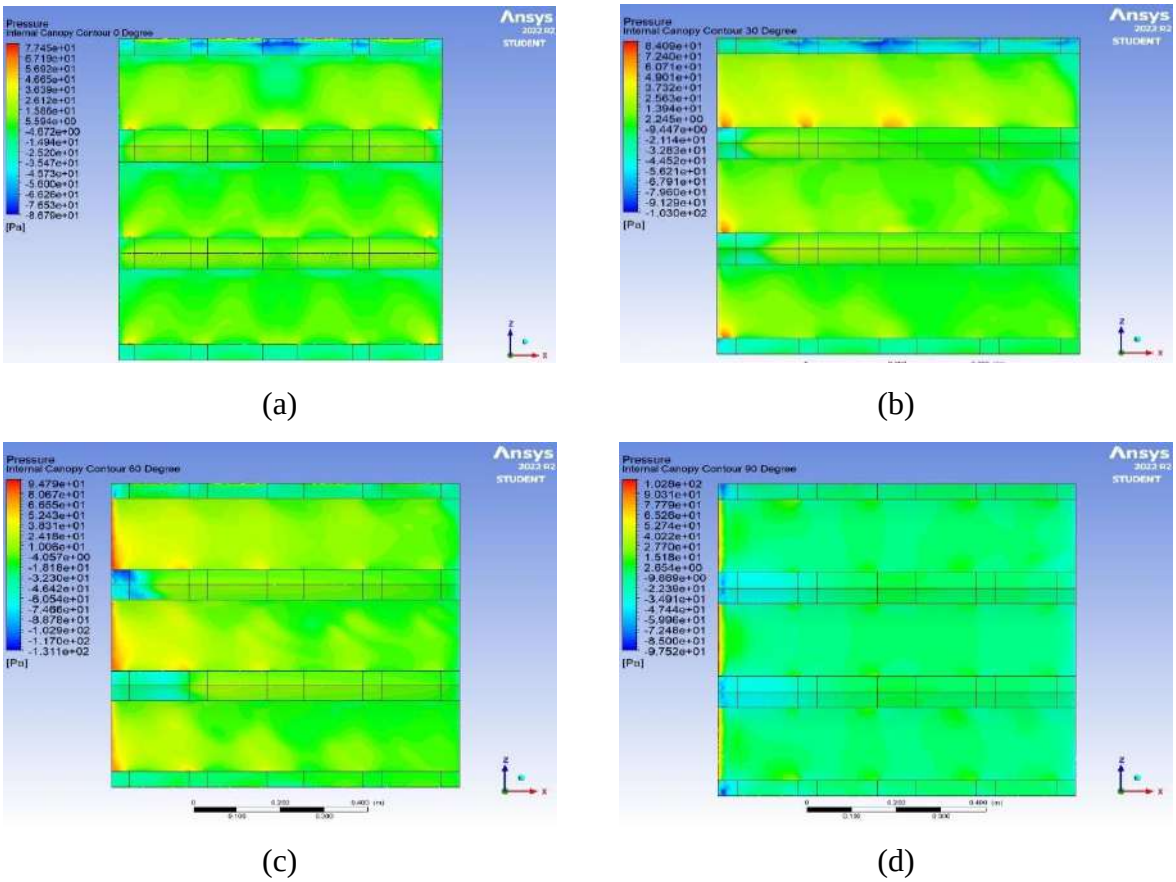

(a) (b)

(c) (d)

Fig. 14. Internal pressure contours for multi-span low-rise structure having apex height of roof as 10 mm. (a) 0° wind incidence, (b) 30° wind incidence, (c) 60° wind incidence, (d) 90° wind incidence.

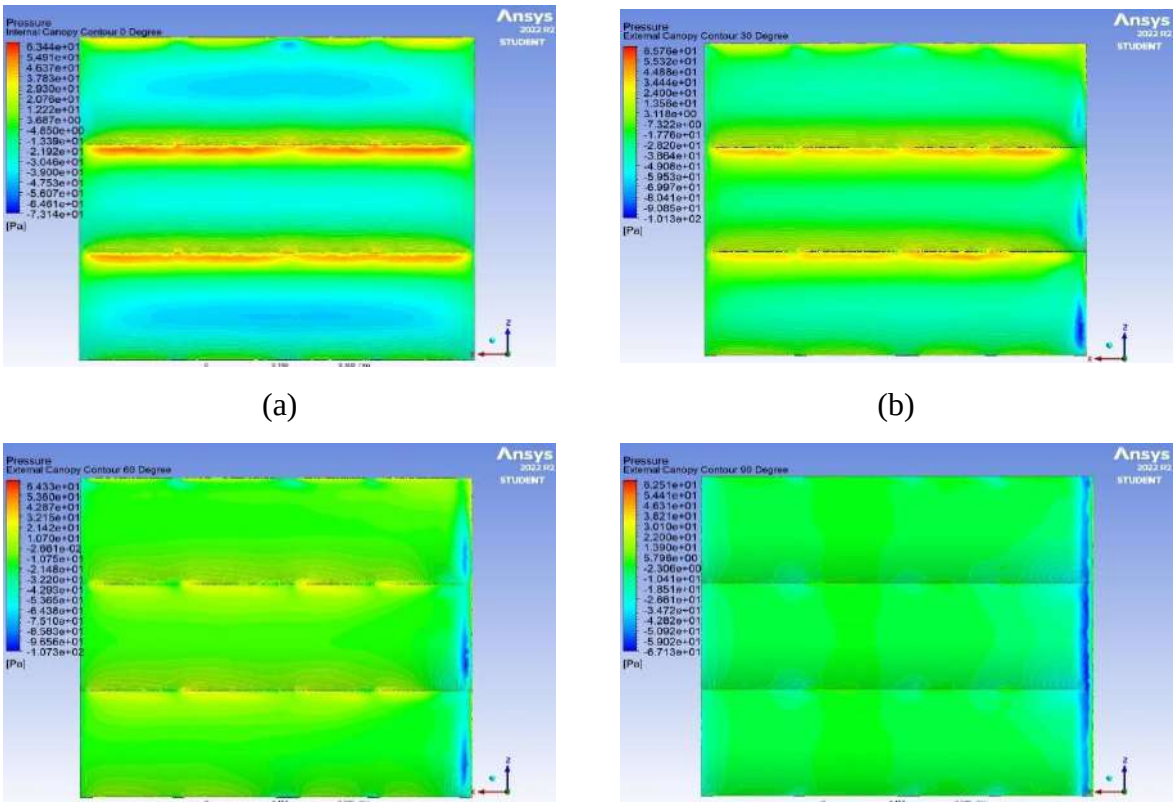

Fig. 15. External pressure contours for multi-span low-rise structure having apex height of roof as 20 mm. (a) 0° wind incidence, (b) 30° wind incidence, (c) 60° wind incidence, (d) 90° wind incidence.

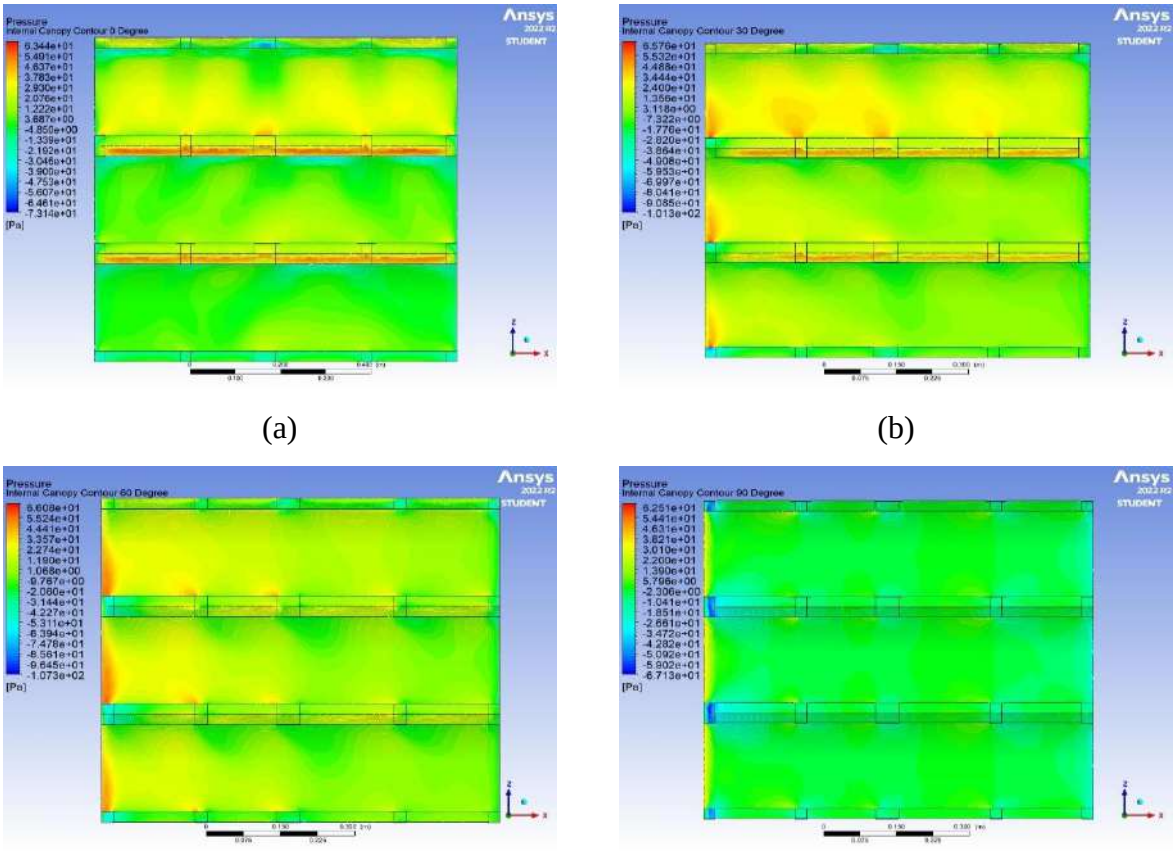

Fig. 16. Internal pressure contours for multi-span low-rise structure having apex height of roof as 20 mm. (a) 0° wind incidence, (b) 30° wind incidence, (c) 60° wind incidence, (d) 90° wind incidence.

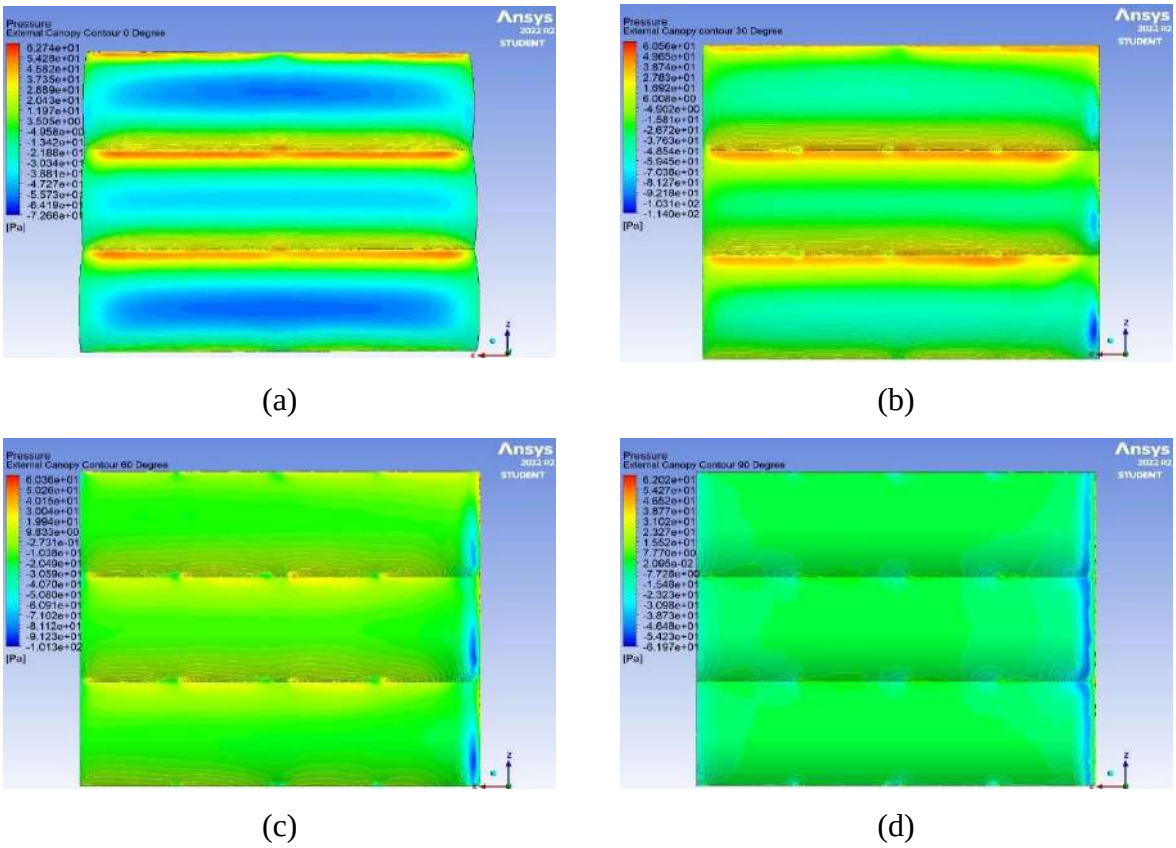

(a) (b)

(c) (d)

Fig. 17. External pressure contours for multi-span low-rise structure having apex height of roof as 30 mm. (a) 0° wind incidence, (b) 30° wind incidence, (c) 60° wind incidence, (d) 90° wind incidence.

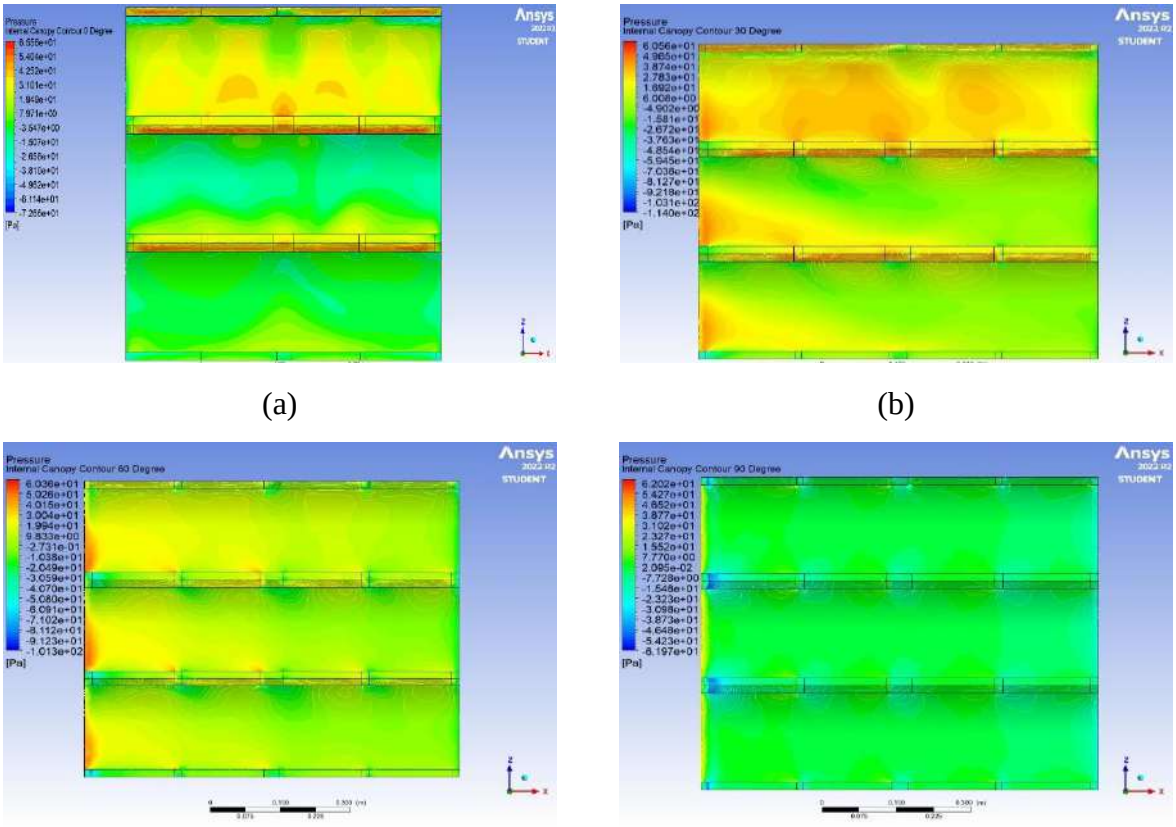

(a) (b)

(c) (d)

Fig. 18. Internal pressure contours for multi-span low-rise structure having apex height of roof as 30 mm. (a) 0° wind incidence, (b) 30° wind incidence, (c) 60° wind incidence, (d) 90° wind incidence.

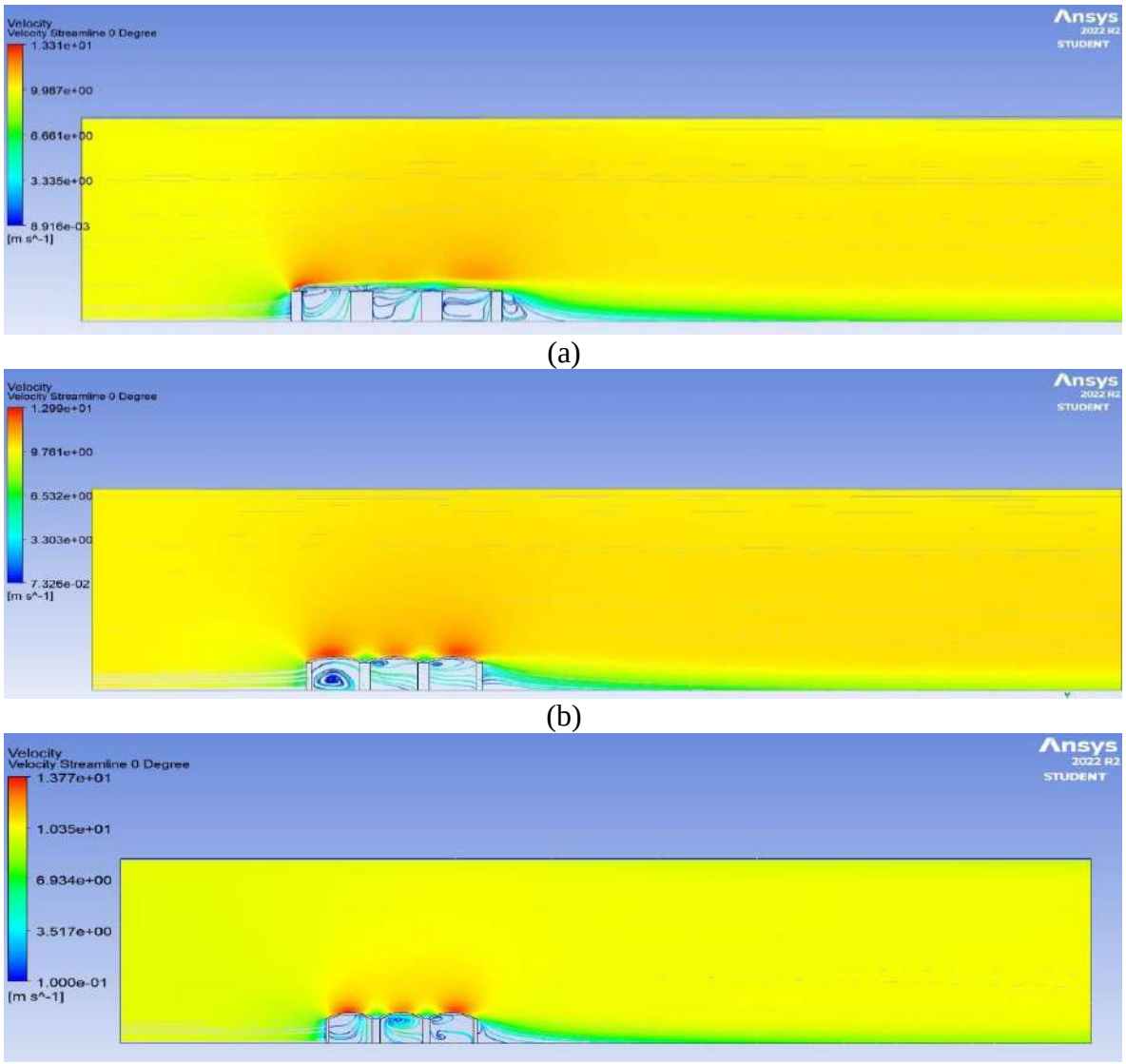

Fig. 19. Velocity streamlines for multi-span low-rise structures. (a) 0° wind incidence, 10 mm apex height model, (b) 0° wind incidence, 20 mm apex height model, (c) 0° wind incidence, 30 mm apex height model.

Overall, the results showed that the apex height of the roof increased, the suction pressure experienced at the top of the first roof also increased. On the lower surface, the magnitude of positive coefficient of pressured increased with increasing apex height. The top surface of the roof experienced suction pressure at all incidence angles, while the lower surface generally experienced positive pressure. In the 20 mm apex height model, the third roof of the building started experiencing suction pressure at 0°. In the model with the 30 mm apex height, both the second and third roofs of the building experienced suction pressure at a wind incidence angle of 0°. The pressure contours for multi-span low-rise structures having varying apex heights are represented in Fig. 13-18. The velocity streamlines for multi-span low-rise structures having varying apex heights are represented in Fig. 19.

In our research, we also plotted the coefficient of pressure against the wind incidence angle for single-span and multi-span low-rise structures with apex heights of 10 mm, 20 mm, and 30 mm. The findings from these graphs, represented in Fig. 20-23, are consistent with the results obtained from the pressure contours and the table.

All these findings have important implications for the design and construction of single-span and multi-span low-rise structures with curved canopy roofs.

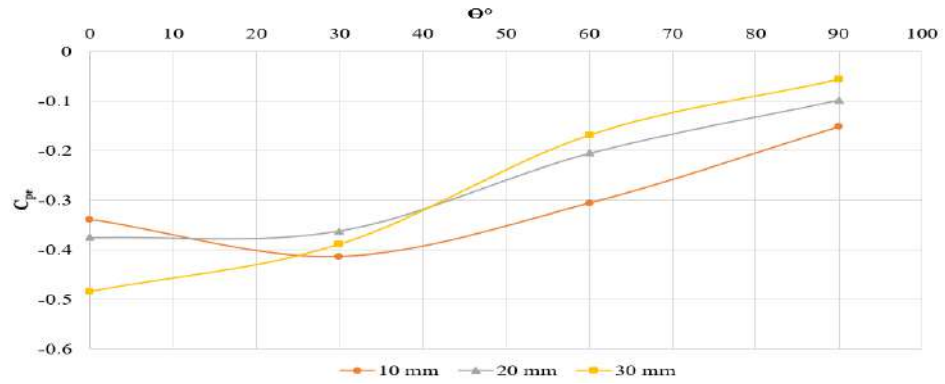

(a)

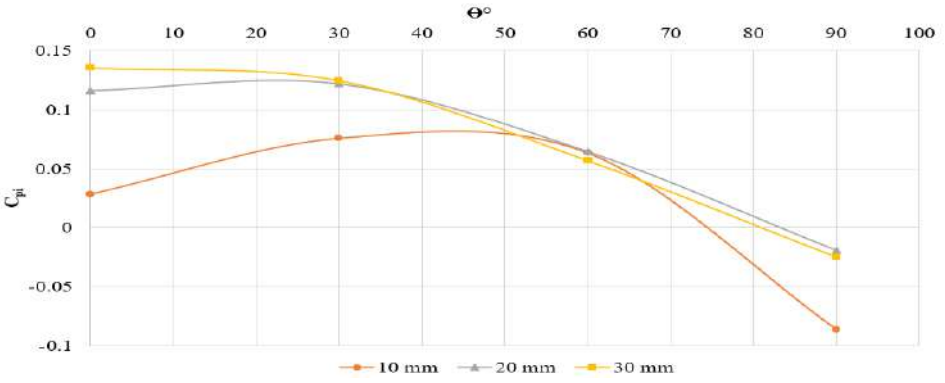

(b)

Fig. 20. Graphs for coefficient of pressure (C_p) v/s wind incidence angle (θ°) for single-span low-rise structure models having varying apex heights. (a) For external contour, (b) for internal contour.

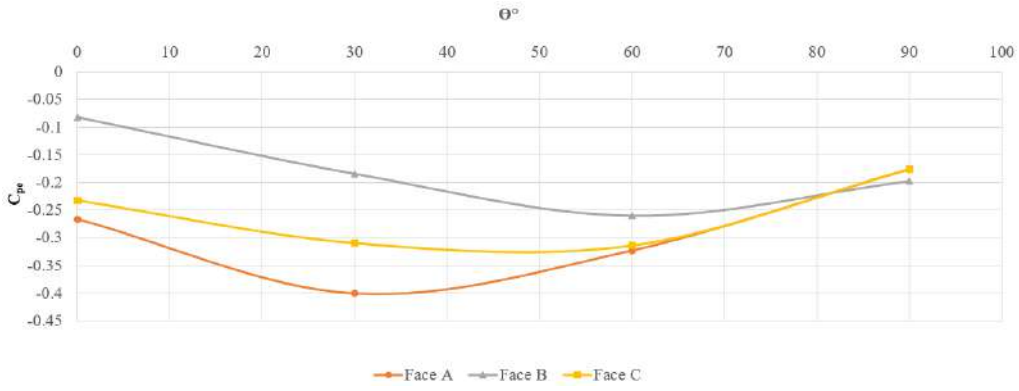

(a)

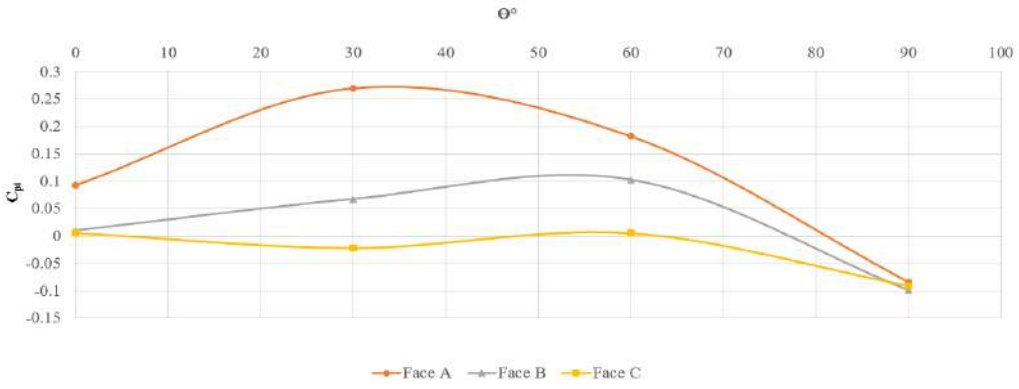

(b)

Fig. 21. Graphs for coefficient of pressure (C_p) v/s wind incidence angle (θ°) for multi-span low-rise structure model having apex height as 10 mm. (a) For external contour, (b) for internal contour.

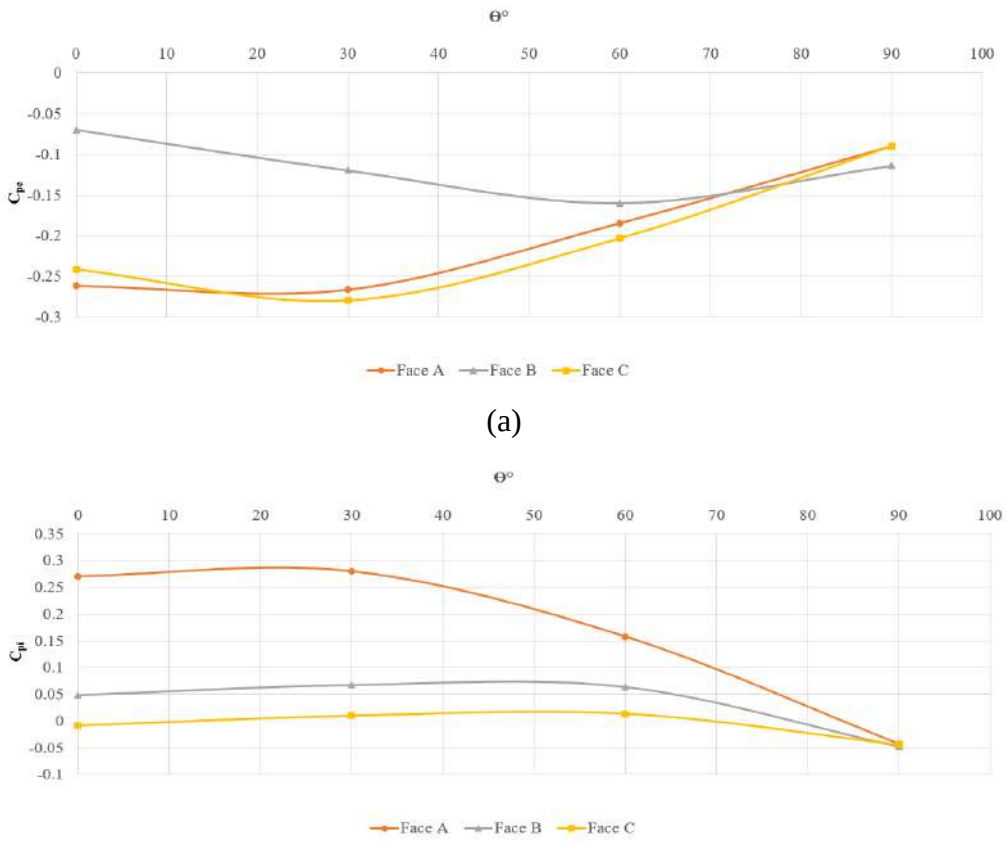

Fig. 22. Graphs for coefficient of pressure (C_p) v/s wind incidence angle (θ°) for multi-span low-rise structure model having apex height as 20 mm. (a) For external contour, (b) for internal contour.

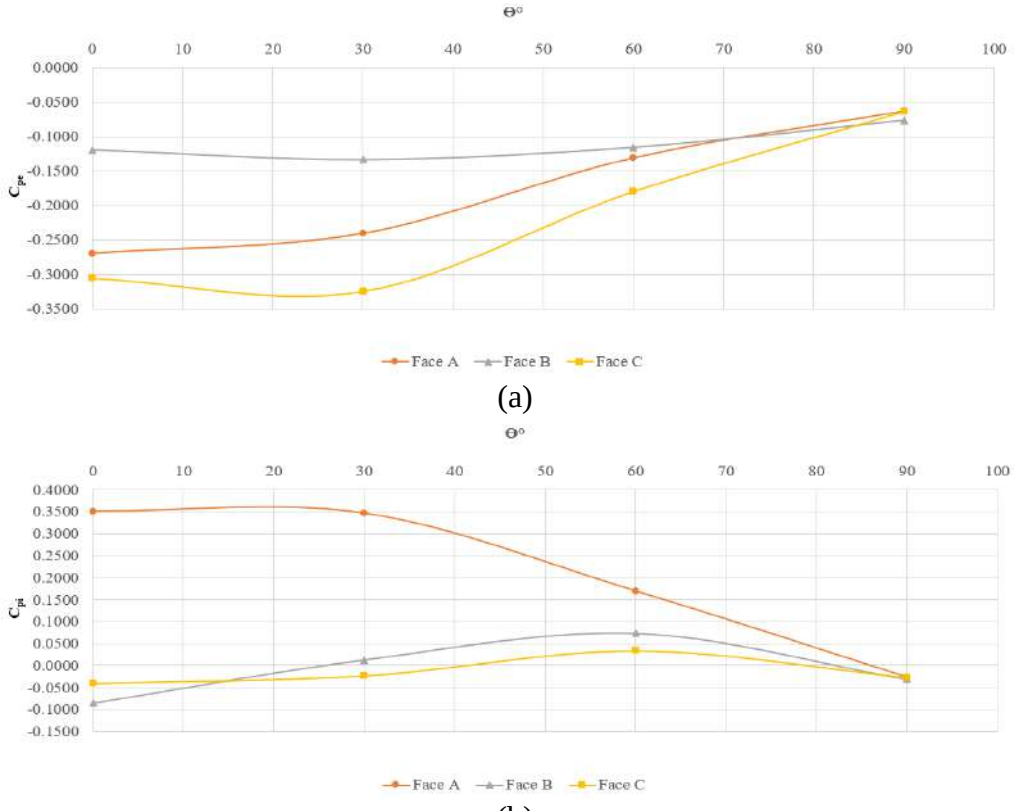

Fig. 23. Graphs for coefficient of pressure (C_p) v/s wind incidence angle (θ°) for multi-span low-rise structure model having apex height as 30 mm. (a) For external contour, (b) for internal contour.

Table 3. C_p values for single-span models having varying apex heights

Angle of Incidence of Wind	C_{pe} (External Contour)	C_{pi} (Internal Contour)
Apex Height of Roof as 10 mm		
0°	-0.3383	0.0285
30°	-0.4138	0.0760
60°	-0.3060	0.0635
90°	-0.1508	-0.0865
Apex Height of Roof as 20 mm		
0°	-0.3756	0.1165
30°	-0.3619	0.1223
60°	-0.2051	0.0646
90°	-0.0973	-0.0192
Apex Height of Roof as 30 mm		
0°	-0.4845	0.1358
30°	-0.3890	0.1249
60°	-0.1687	0.0568
90°	-0.0561	-0.0251

Table 4. C_p values for multi-span model having apex height as 10 mm

Angle of Incidence of Wind	C_{pe} (External Contour)	C_{pi} (Internal Contour)
Face A		
0°	-0.2665	0.0927
30°	-0.4008	0.2695
60°	-0.3230	0.1818
90°	-0.1762	-0.0837
Face B		
0°	-0.0821	0.0097
30°	-0.1842	0.0672
60°	-0.2602	0.1022
90°	-0.1977	-0.0993
Face C		
0°	-0.2325	0.0055
30°	-0.3093	-0.0217
60°	-0.3137	0.0051
90°	-0.1763	-0.0907

Table 5. C_p values for multi-span model having apex height as 20 mm

Angle of Incidence of Wind	C_{pe} (External Contour)	C_{pi} (Internal Contour)
Face A		
0°	-0.2613	0.2704
30°	-0.2662	0.2796
60°	-0.1842	0.1578
90°	-0.0897	-0.0426
Face B		
0°	-0.0698	0.0489
30°	-0.1195	0.0676
60°	-0.1594	0.0638
90°	-0.1138	-0.0477
Face C		
0°	-0.2409	-0.0080
30°	-0.2790	0.0101
60°	-0.2028	0.0139
90°	-0.0900	-0.0433

Table 6. C_p values for multi-span model having apex height as 30 mm

Angle of Incidence of Wind	C_{pe} (External Contour)	C_{pi} (Internal Contour)
Face A		
0°	-0.2695	0.3505
30°	-0.2407	0.3463
60°	-0.1306	0.1692
90°	-0.0624	-0.0270
Face B		
0°	-0.1191	-0.0854
30°	-0.1331	0.0129
60°	-0.1156	0.0731
90°	-0.0763	-0.0314
Face C		
0°	-0.3053	-0.0408
30°	-0.3245	-0.0233
60°	-0.1796	0.0336
90°	-0.0637	-0.0271

6. Conclusion

The results of this study, which used CFD simulations to examine the aerodynamic effects of curved canopy roofs on single-span and multi-span low-rise structures, can be summarized as follows:

- The apex height of the curved canopy roof significantly impacts the distribution of suction pressure on the surface.
- Higher apex heights can provide greater resistance to wind loads and other aerodynamic forces.
- The presence of a curved canopy roof on multi-span low-rise structures significantly affects the aerodynamic forces acting on the structure.
- Increasing the apex height of the canopy roof resulted in an increase in suction pressure experienced at the top of the first roof.
- On the lower surface, the magnitude of positive coefficient of pressure increased with increasing apex height.

The findings of this study are valuable for the design and construction of single-span and multi-span low-rise structures with curved canopy roofs. Further research is needed to investigate the effects of other factors, such as roof slope and aspect ratio, on the aerodynamic performance of single-span and multi-span low-rise structures with curved canopy roofs. The findings of this study can be used to guide the design and construction of multi-span low-rise structures with curved canopy roofs. Additionally, by using similar research methods and conducting thorough CFD simulations, it is possible to examine the aerodynamic effects on other types of roofs and in different wind speed conditions. This would allow for the development of a comprehensive set of guidelines for analyzing the impact of wind on single-span and multi-span structures, which could be incorporated into widely accepted wind codes such as IS 875: Part 3.

Nomenclature

u_i	:	Velocity Component	P	:	Pressure
u_t	:	Eddy Velocity	P_0	:	Reference Pressure
g	:	Acceleration due to gravity	E_{ij}	:	Rate of Deformation
z	:	Height	F	:	Force
C_p	:	Coefficient of Pressure	ρ	:	Density
C_{pe}	:	External Coefficient of Pressure	μ	:	Viscosity
C_{pi}	:	Internal Coefficient of Pressure	∇	:	Divergence
V	:	Speed			

Acknowledgement

The authors acknowledge Delhi Technological University, Delhi, India, for the financial support provided to carry out this research. Our sincere appreciation and gratitude go to the University for their Support

References

[1] A. M. Aly, F. Resta, and A. Zasso, “Active Control in a High-Rise Building under Multidirectional Wind Loads,” in *Structures Congress 2008*, Oct. 2008, pp. 1–10. https://doi.org/10.1061/41016(314)285.

[2] B. W. Yan and Q. S. Li, “Detached-eddy and large-eddy simulations of wind effects on a high-rise structure,” *Comput Fluids*, vol. 150, pp. 74–83, Jun. 2017, https://doi.org/10.1016/j.compfluid.2017.02.009.

[3] Rohit B. Khade and. Prashant M. Kulkarni, “Effect of Wind Load on Structural Performance of Dimensionally Regular and Irregular High rise Buildings with different Outrigger Systems,”

International Journal of Engineering and Management Research, vol. 9, no. 4, pp. 25–29, Aug. 2019, https://doi.org/10.31033/ijemr.9.4.5.

[4] Q. Yan, D. Li, K. Liu, and Y. Bowen, "CFD/FEM Based Analysis Framework for Wind Effects on Tall Buildings in Urban Areas," *DEStech Transactions on Engineering and Technology Research*, no. icia, Nov. 2017, https://doi.org/10.12783/dtetr/icia2017/15668.

[5] S. K. Nagar, R. Raj, and N. Dev, "Proximity effects between two plus-plan shaped high-rise buildings on mean and RMS pressure coefficients," *Scientia Iranica*, vol. 0, no. 0, pp. 0–0, Jul. 2021, https://doi.org/10.24200/sci.2021.55928.4484.

[6] A. M. Aly, "Influence of Turbulence, Orientation, and Site Configuration on the Response of Buildings to Extreme Wind," *The Scientific World Journal*, vol. 2014, pp. 1–15, 2014, https://doi.org/10.1155/2014/178465.

[7] J. H. Oh, G. A. Kopp, and D. R. Inculet, "The UWO contribution to the NIST aerodynamic database for wind loads on low buildings: Part 3. Internal pressures," *Journal of Wind Engineering and Industrial Aerodynamics*, vol. 95, no. 8, pp. 755–779, Aug. 2007, https://doi.org/10.1016/j.jweia.2007.01.007.

[8] H. W. Tieleman, "Problems associated with flow modelling procedures for low-rise structures," *Journal of Wind Engineering and Industrial Aerodynamics*, vol. 42, no. 1–3, pp. 923–934, Oct. 1992, https://doi.org/10.1016/0167-6105(92)90099-V.

[9] R. N. Sharma and P. J. Richards, "The effect of roof flexibility on internal pressure fluctuations," *Journal of Wind Engineering and Industrial Aerodynamics*, vol. 72, pp. 175–186, Nov. 1997, https://doi.org/10.1016/S0167-6105(97)00252-3.

[10] D.-W. Seo and L. Caracoglia, "Derivation of equivalent gust effect factors for wind loading on low-rise buildings through Database-Assisted-Design approach," *Eng Struct*, vol. 32, no. 1, pp. 328–336, Jan. 2010, https://doi.org/10.1016/j.engstruct.2009.07.020.

[11] A. Gupta, T. Stathopoulos, and P. Saathoff, "Wind tunnel investigation of the downwash effect of a rooftop structure on plume dispersion," *Atmos Environ*, vol. 46, pp. 496–507, Jan. 2012, https://doi.org/10.1016/j.atmosenv.2011.08.039.

[12] A. F. Akon and G. A. Kopp, "Mean pressure distributions and reattachment lengths for roof-separation bubbles on low-rise buildings," *Journal of Wind Engineering and Industrial Aerodynamics*, vol. 155, pp. 115–125, Aug. 2016, https://doi.org/10.1016/j.jweia.2016.05.008.

[13] P. Zhao, H. Dong, and J. Sui, "Numerical Simulation of Surface Wind Pressures on Low-Rise Buildings," *Applied Mechanics and Materials*, vol. 353–356, pp. 3545–3548, Aug. 2013, https://doi.org/10.4028/www.scientific.net/AMM.353-356.3545.

[14] D. Surry and J. X. Lin, "The effect of surroundings and roof corner geometric modifications on roof pressures on low-rise buildings," *Journal of Wind Engineering and Industrial Aerodynamics*, vol. 58, no. 1–2, pp. 113–138, Oct. 1995, https://doi.org/10.1016/0167-6105(95)00016-K.

[15] M. Kalra, P. Bajpai, and D. Singh, "Effect of Wind on Multi Storey Buildings of Different Shapes," *Indian J Sci Technol*, vol. 9, no. 48, Dec. 2016, https://doi.org/10.17485/ijst/2016/v9i48/105705.

[16] M. Asghari Mooneghi and R. Kargarmoakhar, "Aerodynamic Mitigation and Shape Optimization of Buildings: Review," *Journal of Building Engineering*, vol. 6, pp. 225–235, Jun. 2016, https://doi.org/10.1016/j.jobe.2016.01.009.

[17] Q. M. Zahid Iqbal and A. L. S. Chan, "Pedestrian level wind environment assessment around group of high-rise cross-shaped buildings: Effect of building shape, separation and orientation," *Build Environ*, vol. 101, pp. 45–63, May 2016, https://doi.org/10.1016/j.buildenv.2016.02.015.

[18] Y. Yuan, Y. Dai, and S. Jiang, "Experimental Study of Wind Pressure Correlation and Spectrum Characteristics on the Surface of Rectangular Roof Structure," *DEStech Transactions on Computer Science and Engineering*, no. aicae, Oct. 2019, https://doi.org/10.12783/dtcse/aicae2019/31499.

[19] Shuifu Chen and Xiaoping Wu, "Numerical study of wind-driven rain distribution on low-rise buildings with different roof styles," in *2011 International Conference on Electric Technology and Civil Engineering (ICETCE)*, Apr. 2011, pp. 3282–3285. https://doi.org/10.1109/ICETCE.2011.5774637.

[20] J. Singh and A. K. Roy, "Wind Pressure Coefficients on Pyramidal Roof of Square Plan Low Rise Double Storey Building," *Computational Engineering and Physical Modeling*, vol. 1, no. 1, pp. 1–16, 2019, https://doi.org/10.22115/cepm.2019.144599.1043.

[21] D. JIeMIN and H. Zhijun, "Characteristics of wind load and wind resistant design of membrane structure canopy roof of large-scale stadium," in *Fourth International Conference on Advances in Steel Structures*, Elsevier, 2005, pp. 1783–1788. https://doi.org/10.1016/B978-008044637-0/50266-3.

[22] M. Llaguno-Munitxa, E. Bou-Zeid, and M. Hultmark, "The influence of building geometry on street canyon air flow: Validation of large eddy simulations against wind tunnel experiments," *Journal of Wind Engineering and Industrial Aerodynamics*, vol. 165, pp. 115–130, Jun. 2017, https://doi.org/10.1016/j.jweia.2017.03.007.

[23] J. Colliers, M. Mollaert, J. Degroote, and L. de Laet, "Prototyping of thin shell wind tunnel models to facilitate experimental wind load analysis on curved canopy structures," *Journal of Wind Engineering and Industrial Aerodynamics*, vol. 188, pp. 308–322, May 2019, https://doi.org/10.1016/j.jweia.2019.03.004.

[24] T. Kurabuchi, M. Ohba, T. Endo, Y. Akamine, and F. Nakayama, "Local Dynamic Similarity Model of Cross-Ventilation Part 1 - Theoretical Framework," *International Journal of Ventilation*, vol. 2, no. 4, pp. 371–382, Apr. 2004, https://doi.org/10.1080/14733315.2004.11683679.

[25] G. Portela and L. A. Godoy, "Wind pressure and buckling of grouped steel tanks," *Wind and Structures*, vol. 10, no. 1, pp. 23–44, Feb. 2007, https://doi.org/10.12989/was.2007.10.1.023.

[26] Y. G. Wang, Z. N. Li, B. Gong, and Q. S. Li, "Wind Pressure and Wind-Induced Vibration of Heliostat," *Key Eng Mater*, vol. 400–402, pp. 935–940, Oct. 2008, https://doi.org/10.4028/www.scientific.net/KEM.400-402.935.

[27] J. W. Tang, Y. M. Xie, P. Felicetti, J. Y. Tu, and J. D. Li, "Numerical simulations of wind drags on straight and twisted polygonal buildings," *The Structural Design of Tall and Special Buildings*, vol. 22, no. 1, pp. 62–73, Jan. 2013, https://doi.org/10.1002/tal.657.

[28] D. S. K. Verma, A. K. Roy, S. Lather, and M. Sood, "CFD Simulation for Wind Load on Octagonal Tall Buildings," *International Journal of Engineering Trends and Technology*, vol. 24, no. 4, pp. 211–216, Jun. 2015, https://doi.org/10.14445/22315381/IJETT-V24P239.

[29] S. Muffassir and L. G. Kalurkar, "Comparative Study on Wind Analysis of Multi-story RCC and Composite Structure for Different Plan Configuration," *IOSR Journal of Mechanical and Civil Engineering*, vol. 13, no. 04, pp. 42–49, Apr. 2016, https://doi.org/10.9790/1684-1304074249.

[30] L. James Lo, D. Banks, and A. Novoselac, "Combined wind tunnel and CFD analysis for indoor airflow prediction of wind-driven cross ventilation," *Build Environ*, vol. 60, pp. 12–23, Feb. 2013, https://doi.org/10.1016/j.buildenv.2012.10.022.

[31] *IS 875 (Part 3), "Design Loads (Other than Earthquake) for Buildings and Structures-Code of Practice Part 3 Wind Loads (Third Revision)." 2015.*

[32] J. Franke *et al.*, "Recommendations on the Use of CFD In Wind Engineering." [Online]. Available: http://www.costc14.bham.ac.uk/

[33] "ANSYS Meshing User's Guide, Release 13.0. Canonsburg: ANSYS, Inc., 2010."